DUAL TOPOLOGICAL UNITARIZATION: AN ORDERED APPROACH TO HADRON THEORY

Geoffrey F. CHEW

Department of Physics and Lawrence Berkeley Laboratory, University of California, Berkeley, California 94720, U.S.A.

and

Carl ROSENZWEIG

Department of Physics, Syracuse University, Syracuse, New York 13210, U.S.A.

NORTH-HOLLAND PUBLISHING COMPANY – AMSTERDAM

PHYSICS REPORTS (Section C of Physics Letters) 41, No. 5 (1978) 263–327. NORTH-HOLLAND PUBLISHING COMPANY

DUAL TOPOLOGICAL UNITARIZATION: AN ORDERED APPROACH TO HADRON THEORY*†

Geoffrey F. CHEW

Department of Physics and Lawrence Berkeley Laboratory, University of California, Berkeley, California 94720, U.S.A.

and

Carl ROSENZWEIG

Department of Physics, Syracuse University, Syracuse, New York 13210, U.S.A.

Received 15 December 1977

Contents:

Abstract:

A review is given of developments between 1973 and 1977 that have added the concept of order to general S-matrix principles with the aim of constructing a bootstrap theory of hadrons.

* Work supported in part by the U.S. Department of Energy under Contracts W-7405 ENG-48 and EY-76-S-02-3533.

1. Introduction

In 1973 there began an S-matrix approach to strong interactions, based on a combination of unitarity, topology and Regge behavior, that stirred widespread interest by generating certain of the predictions characteristic of quark models while showing the power to go beyond these models. The approach evolved from the dual models of the late sixties but was qualitatively distinct in recognizing unitarity from the start as an essential constraint. Chan Hong-Mo and collaborators [1, 2] have dubbed the new approach "dual unitarization", while Veneziano [3] has called it the "topological expansion". The adjective "topological" recognizes the need to distinguish order from disorder – a central feature of the new approach. Four years of work on dual topological unitarization (DTU) have produced results sufficiently encouraging as now to warrant a review article. Our survey here will describe the general picture as it appears on July 1, 1977. Readers should bear in mind that the field has not reached a state of maturity and that by the time they see this article there may have occurred further important developments.

To capture the attention of readers not already impressed by the potentialities of a topological investigation of unitarity, we call immediate attention to the celebrated but mysterious Okubo-Zweig-Iizuka (OZI) rule. The approach characterized as DTU not only generates this rule but gives a quantitative account of the extent to which the rule is broken. The accuracy of the rule is related to other approximate hadronic regularities such as the limitation of transverse momenta, the short-range character of rapidity correlations, the absence of exotics and the exchange degeneracy of leading Regge trajectories. All these manifestations of regularity within the hadron S matrix, as well as others less well recognized, are seen in the DTU approach as different facets of a single principle of order. Imperfections in order – a degree of disorder – is seen as an inevitable consequence of unitarity. No arbitrary parameters (such as a gluon coupling constant) are needed in DTU to determine the magnitude of imperfection.

Rather than following an historical line in this review we shall proceed from general S-matrix principles, seeking their satisfaction by starting from an approximation where the degree of order is maximized. To the extent that we speak of "quarks" the concept is not postulated but deduced as a manifestation of order. Our rules for quark-line diagrams will nevertheless turn out to be the same as those in approaches where quarks are inserted ab initio. Readers need not share the bootstrap viewpoint in order to follow our presentation. The bulk of our review is restricted to the meson sector of the S matrix, the extension of topological analysis to baryons and baryonium being recent and incompletely understood. We shall see that for mesons the DTU approach appears remarkably satisfactory.

Because the injection of order and or topology into hadron theory is a new departure, we cannot derive the essential DTU concepts. The reader should regard these concepts as motivated by the experimental observation of order in hadronic phenomena and justified by mathematical self consistency. According to the bootstrap hypothesis the nonlinear constraints of unitarity on a Poincaré-invariant analytic S matrix are so demanding as to determine the S matrix uniquely. The human mind is not sufficiently powerful to find this unique solution without hints from experiment, and different approaches have in the past seized on different hints as a guide. The DTU approach focuses on order as its signpost.

Maximal order is represented through the concept of "planar S matrix", a fundamental notion developed in section 2 in a form suitable only to mesons but which may be generalized to include baryons. Section 3 develops special internal-quantum-number consequences for the meson sector,

and section 4 interrupts the theoretical argument to survey the extent to which experimentally-observed mesons are approximately "planar". Having drawn attention to the strikingly planar appearance of the meson sector, we proceed in section 5 to develop the S-matrix topological expansion – intended to correct systematically the failure of the planar S matrix to satisfy unitarity. The successive terms of the topological expansion correspond to successively-increasing disorder, the planar S matrix being the leading term. The concepts of handles and boundaries as measures of disorder are introduced in section 5.

Section 6 describes a peripheral mechanism tending to suppress topological-expansion components as their complexity increases, while section 7 is concerned with an entirely different convergence mechanism related to internal quantum numbers. Section 8 discusses the renormalization of planar S-matrix poles that results from the higher terms of the topological expansion.

The general portion of our review concludes with section 8 and we then turn to a variety of models that are based on the general principles but that attempt quantitative predictions through simplifying approximations. Section 9 describes a multiperipheral bootstrap model that determines positions and couplings of leading planar Regge trajectories at moderate values of $|t|$. Section 10 describes a corresponding moderate-$|t|$ model of the leading corrections to the planar components of the topological expansion – with emphasis on the pomeron picture that emerges. Section 10 discusses the subtle relation between SU_N symmetry breaking and cylinder violations of planar order. In section 11 we consider OZI-rule violation, and in section 12 models of single-handle (torus) components are described, with application to ρ–A_2 splitting. Efforts to incorporate baryons and baryonium into the DTU approach will be described in section 13.

The reader of this review is assumed to feel comfortable with standard analytic S-matrix theory at the level, say, of the monographs by Martin and Spearman [4] or Collins and Squires [5]. If terms such as "cluster-decomposition", "connected part", "crossing", or "discontinuity" are not familiar, there will be difficulty in following our presentation. We do not, however, assume any knowledge of topology. Those aspects of duality which are relevant to our discussion can be found in a recent review by Fukugita and Igi [6].

2. The planar S matrix; external regularities

The notion of maximal order within the S-matrix framework is realized through the so-called "planar S matrix". The concept of planar S matrix has not been "derived", it has been motivated by experimental facts and is justified by self consistency [1–3]. The planar idea grew out of dual models but as we use it is not equivalent. Readers who feel the need for experimental motivation may scan section 4, which surveys the observed approximate meson regularities supporting planarity as a useful physical idea.

The sequentially-ordered S matrix

Planarity is so closely related to order that we proceed by immediately introducing the artificial, but profoundly useful notion of a sequentially-ordered Hilbert space. A physical channel is entirely specified by giving the momentum, spin and type of each particle. In our ordered Hilbert space specification of an ordered channel requires additionally that particles be assigned positions in a sequence. For each N-particle physical channel there are $N!$ ordered channels, so our ordered Hilbert space is larger than the physical Hilbert space.

We may formally represent an ordered asymptotic state by a bra or ket column vector

$$\left|\begin{matrix} A_1 \\ A_2 \\ \vdots \end{matrix}\right\rangle , \quad \left\langle\begin{matrix} A_1 \\ A_2 \\ \vdots \end{matrix}\right|$$

where A_i denotes the type, momentum and helicity of the ith particle in the sequence. Within the ordered Hilbert space we can define an S matrix connecting the ordered asymptotic states. We call this the ordered S matrix and symbolize it as S_0. Elements of the ordered S matrix may then be represented graphically by fig. 2.1. Although a similar pictorial representation is often used for physical S-matrix elements, the ordering of particles there is irrelevant. Particle ordering is needed even for the physical S matrix in the discussion of statistics but channels which differ merely in particle order are physically equivalent – the corresponding asymptotic wave functions and S-matrix elements being equal up to phase factors. For the ordered S matrix introduced here, changes of particle order generally change the modulus of an element as well as the phase.

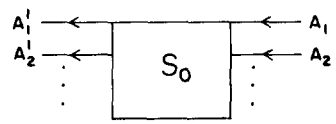

Fig. 2.1. An element of the ordered S matrix.

The ordered S matrix, whose elements we depict in fig. 2.1, is supposed to be unitary *with respect to the space of ordered states.* That is,

$$S_0^+ S_0 = S_0 S_0^+ = 1, \tag{2.1}$$

with

$$1 = \sum_{A,B,C,\ldots} \left|\begin{matrix} A \\ B \\ C \\ \vdots \end{matrix}\right\rangle \left\langle\begin{matrix} A \\ B \\ C \\ \vdots \end{matrix}\right| . \tag{2.2}$$

The property of unitarity for S_0 guarantees a consistent (factorizable) particle spectrum on which the DTU approach can be based. Achievement of such a base is the chief reason for introducing the ordered S matrix.

There must of course be a rule for connecting the ordered S matrix to physical observations – in effect contracting the Hilbert space of asymptotic states. In section 5 we shall find this rule to be expressible through a "topological expansion", in which a "planar S matrix" emerges as the leading component, elements of the planar S matrix being linearly related to elements of the ordered S matrix. (It will quickly be seen why the adjective "planar" is appropriate.) Planar S-matrix elements do not depend on particle order and may be compared to experiment. At the same time, because of the linear connection with elements of the ordered S matrix, certain striking regularities are present. Enough of these "planar regularities" have been approximately verified by experimental observation (see section 4) to suggest that the leading component of the topological expansion – the planar S matrix – is interestingly close to the physical S matrix.

Roughly speaking, characteristic planar regularities may be divided into two categories: those associated with internal quantum numbers and those associated with momentum and spin (including T, C and P). We shall refer to the former regularities as "internal" and to the latter as "external". The present section will confine itself to external planar regularities, while section 3 will discuss internal aspects of planarity – where the connection with the quark concept begins to emerge.

Ordered connected parts; ordered crossing

We assume a cluster decomposition of the ordered S matrix, using "ring" diagrams to denote ordered connected parts as in the example of fig. 2.2. The order of lines around each ring is important, in contrast to the "bubble" diagrams for physical connected parts, which look similar. We

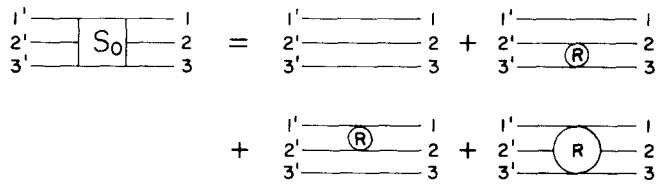

Fig. 2.2. Cluster decomposition of the ordered S matrix.

introduce the explicit symbol R to remind the reader of this distinction. The essential feature in ordered cluster decomposition is that particle lines drawn in a plane never cross each other. For example we do not admit decompositions of the form shown in fig. 2.3. We shall find a similar character for the pictorial representation of ring products that arise in expressing unitarity for the ordered S matrix; on a planar surface no particle lines need cross. Ordering, in other words, is closely related to planarity.

Fig. 2.3. Nonadmissible decompositions of S_0.

Assuming ordered connected parts to be analytic functions of particle momenta, one may deduce an "ordered crossing" property that relates certain continuations from positive to negative energy with the replacement of ingoing particles by outgoing antiparticles (or vice versa) [7]. Ordered crossing follows from the unitarity of S_0 in the same way that regular crossing follows from the unitarity of S. The difference is that each cyclic permutation of particle lines in a ring connected-part represents a distinct analytic function, and only those crossings within a given ring that maintain the cyclic permutation correspond to elements of the ordered S matrix.

Consider for example the analytic function corresponding to the four-line ordered ring diagram of fig. 2.4. By suitably choosing which energies are positive and which are negative this single analytic function corresponds to the four ordered transitions such as $\left|\begin{matrix}A\\B\end{matrix}\right\rangle \rightarrow \left\langle\begin{matrix}\overline{D}\\\overline{C}\end{matrix}\right|$, shown in fig.

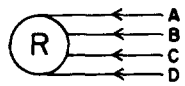

Fig. 2.4. A four line, ordered, ring diagram.

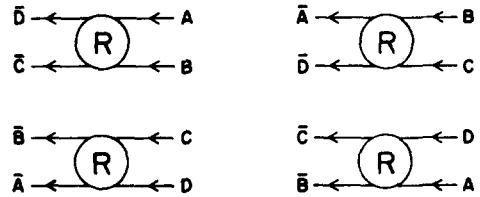

Fig. 2.5. Four ordered transitions related by ordered crossing.

2.5, but does *not* correspond to transitions between ordered channels containing particles (A, C) and (B, D). The latter transitions correspond to different analytic functions associated with different ring diagrams.

We may use figs. 2.4 and 2.5 to explain a phase convention needed when fermions are present. Even though our simple sequential ordering must be generalized in order to handle baryons, the basic idea behind the following rule will survive. If a fermion line is crossed twice in the same sense (say clockwise) a minus sign can be shown to result [8]. Thus, for example, if particle D is a fermion, we have the relation of fig. 2.6. We shall employ the convention that a reversal of sign occurs when a fermion is crossed *at the top* of the ring, with no sign change when a fermion crosses at the bottom. Because the total number of fermion lines is necessarily even, such a convention can be shown to be consistent [9, 10]. Suppose that particles C and D in fig. 2.4 are fermions, with A and B bosons. Our convention then says that the first three amplitudes of fig. 2.5 are the analytic continuations of fig. 2.4 with a positive sign, while the remaining amplitude of fig. 2.5 carries a minus sign.

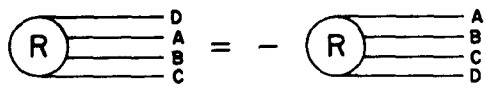

Fig. 2.6. Ordered crossing relationship if D is a fermion.

In section 5 ordered connected parts will constitute the vertices from which the topological expansion is constructed. Let us next consider the poles of ordered connected parts, which in section 5 will allow a physical meaning for lines connecting vertices.

Planar poles

The same unitarity considerations that imply factorizable poles for physical connected parts, with a correspondence between poles and external particles, lead to a similar pole structure for ordered connected parts. Each of the two factors in the residue of a pole in an ordered connected part is itself an ordered connected part. Figure 2.7 gives examples of poles in the connected part

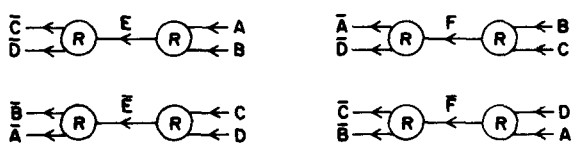

Fig. 2.7. Poles in the ordered connected part of fig. 2.4.

of fig. 2.4 corresponding to the different channels of fig. 2.5. Here the residue factors are 3-line ordered connected parts; as such they possess the ordered crossing property. Note that a pole, if regarded as a single-particle channel in the ordered Hilbert space, is not itself characterized by an order. For this reason it will be possible to attempt a direct correspondence between physical particles – the poles of the physical S matrix – and poles of the ordered S matrix, which we shall call "planar particles". The two sets of poles are different but there must exist some degree of correspondence or there would be no point in discussing the ordered S matrix. Section 4 deals with the question of which physically-observed hadrons may be described as "approximately planar".

Assuming that *some* physical particles correspond at least roughly to certain planar particles, one may seek to define a "planar S matrix" whose poles are those of the ordered S matrix (i.e. the planar poles) but whose multiparticle channels have no order. Elements of such an S matrix might then be compared with experiment.

Construction of the planar S matrix from ordered connected parts

We define the planar S matrix by giving a rule for constructing its connected parts from ordered connected parts. Each N-line connected part of the planar S matrix is a linear superposition of the $(N-1)!$ different ordered connected parts that involve the corresponding planar particles. This operation effectively contracts the ordered Hilbert space. The relative coefficients in the superposition are ± 1 according to whether an even or an odd number of fermion transpositions is involved [10]. Thus, in our 4-line example, with C and D fermions while A and B are bosons, the planar connected part is given by the six-term superposition in fig. 2.8. Such a superposition makes equivalent all particle orderings, up to a ± 1 phase factor, and one sees that the spin-statistics rule for identical particles is satisfied. Full crossing is evidently achieved for planar connected parts.

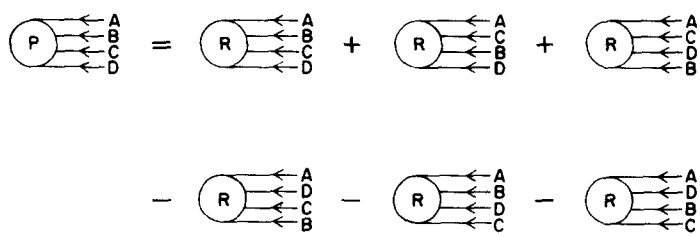

Fig. 2.8. A planar connected part defined as a superposition of ordered connected parts.

Furthermore, although not quite so evident, a consistent pole structure is maintained [10]. It can be shown that superposition, according to the rule illustrated in fig. 2.8, leads to factorizable residues of the poles in planar connected parts – with factors which are themselves planar connected parts. For example, corresponding to fig. 2.7 the 4-line planar connected-part poles could be represented as in fig. 2.9, where the 3-line connected-part residue factors are given by superpositions of the type illustrated in fig. 2.10.

Unitarity

Now, if planar connected parts have correct symmetry and crossing properties and possess a consistent factorizable pole structure, what is inadequate about the planar S matrix? The answer

Fig. 2.9. Poles in a planar connected part.

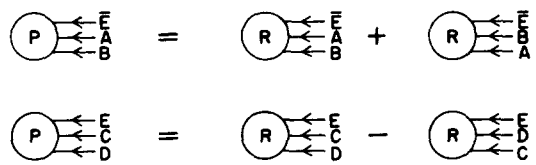

Fig. 2.10. Residue factors of planar, three line connected part.

is, unitarity. If one builds a planar S matrix out of planar connected parts, one finds unitarity not satisfied – even though the ordered S matrix in the *larger* Hilbert space of ordered asymptotic states *is* unitary. The contraction rule illustrated by fig. 2.8 fails to preserve unitarity.

The defect may already be seen in 4-line connected parts. Suppose we consider for a physical $(A, B) \to (\bar{C}, \bar{D})$ amplitude the normal-threshold discontinuity in the variable $s = s_{AB} = s_{CD} = (p_A + p_B)^2 = (p_C + p_D)^2$, associated with a two-particle intermediate channel (E, F). Unitarity implies a formula corresponding to fig. 2.11, where the bubble diagrams carry no meaning for particle ordering. (The + and − designation indicates that the two members of the product are to be evaluated on opposite sides of the cut in question. We shall always understand such a rule for unitarity products and shall henceforth omit the + and − symbols.) We now show, as indicated in fig. 2.12, that the formula of fig. 2.11 is *not* satisfied by planar connected parts.

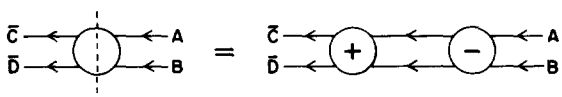

Fig. 2.11. Physical unitarity relationship. Bubble diagrams carry no information about ordering.

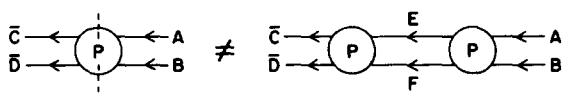

Fig. 2.12. Graphical statement of the fact that planar connected parts do not satisfy unitarity.

Let us start by taking the s-discontinuity in question, term by term within the 6-term superposition of fig. 2.8. We find a superposition of four ordered s-discontinuities, as shown in fig. 2.13. The remaining two terms in fig. 2.8 lack any s discontinuity because they cannot be crossed so as to connect s channels of the ordered S matrix. This property, crucial to the DTU approach, will be derived more systematically in section 5. Let us next consider the rule implied by unitarity of the ordered S matrix for the discontinuities of ordered connected parts. The rule is similar to that of

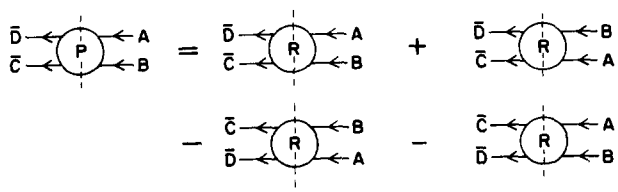

Fig. 2.13. The s discontinuity of fig. 2.8.

fig. 2.11 except that particle ordering is everywhere meaningful. Figure 2.14 gives an example. The important feature is that particle lines never cross in ordered discontinuity products; ordered discontinuities, in other words, are planar products.

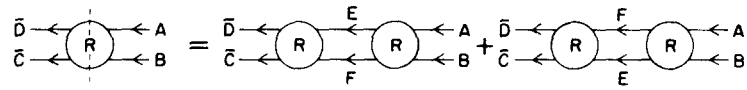

Fig. 2.14. Two-particle discontinuity of an ordered connected part implied by the unitarity of the ordered S matrix. Compare to fig. 2.11.

If the formulas like that of fig. 2.14 are substituted into the equation of fig. 2.13, we find $2 \times 4 = 8$ different planar products of ordered amplitudes making up the discontinuity of the planar connected part in question, i.e. the left-hand side of fig. 2.12. On the other hand, were each member of the product on the right hand in fig. 2.12 expressed as a superposition of six (6) ordered connected parts, we should find $6 \times 6 = 36$ different products. Eight of these would indeed be planar products, but there would be in addition $36 - 8 = 28$ nonplanar products – examples of which are shown in fig. 2.15. Because of these nonplanar components of the right-hand side of fig. 2.12, the left- and right-hand sides cannot be equal; the planar S matrix cannot be unitary.

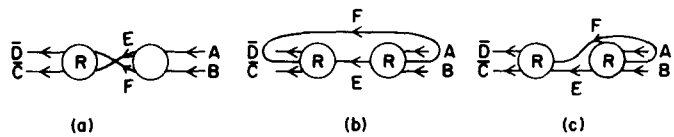

Fig. 2.15. Examples of nonplanar products present on the right-hand side of fig. 2.12.

It will be the task of sections 5, 6 and 7 to show the sense in which nonplanar discontinuity products are smaller than their planar counterparts, so that the planar S matrix has a chance of approximating experiment. Section 5 develops a systematic expansion for calculating the physical S matrix starting with the planar S matrix, based on the necessity of achieving unitarity for the physical S matrix.

The absence of nonplanar discontinuity products leads to planar S-matrix regularities not present in the full S matrix. But unitarity of the ordered S matrix, from which the planar S matrix is constructed, still implies an infinite set of nonlinear relations between ordered connected parts. To the extent that solutions of these relations may not exist, there is no proof that an ordered analytic unitary S matrix exists, just as there is no existence proof for a physical unitary analytic S matrix. In order to proceed we are forced to *assume* the existence of an ordered analytic S matrix with planar discontinuity formulas for its connected parts.

Charge conjugation in the ordered S matrix

Crossing implies that for every planar particle there exists a corresponding planar antiparticle. TCP equivalence of the two ordered amplitudes in fig. 2.16 then requires that the charge conjugation of an arbitrary ordered channel

$$\begin{pmatrix} A \\ B \\ \cdot \\ \cdot \\ \cdot \end{pmatrix} \quad \text{be} \quad \begin{pmatrix} \cdot \\ \cdot \\ \cdot \\ \bar{B} \\ \bar{A} \end{pmatrix},$$

Fig. 2.16. *TCP* equivalence of two ordered amplitudes.

that is, a channel where each particle has been replaced by the corresponding antiparticle and the order has been inverted [10]. For ordered connected parts charge conjugation invariance thus means that, when particles are replaced by antiparticles and the cyclic order is reversed, as indicated by the example of fig. 2.17, the value of the connected part is unchanged up to a phase factor.

Self-conjugate planar particles will be important to certain of our subsequent arguments. Each such particle is characterized by being either even or odd under charge conjugation. That is, in the notation of a single-particle channel

$$(\bar{\mathrm{I}}) = C_{\mathrm{I}}(\mathrm{I}), \qquad \text{where} \qquad C_{\mathrm{I}} = \pm 1. \tag{2.3}$$

It follows that an ordered connected part involving only self-conjugate particles has the property shown in fig. 2.18. That is, inversion of order is equivalent to multiplication by the overall product of charge-conjugation symmetry factors [11, 12]. This rule will turn out in section 10 to be of practical importance, especially when generalized to ordered connected parts involving ordered reggeons.

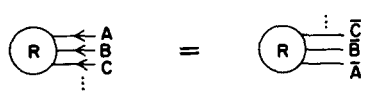

Fig. 2.17. Charge conjugation invariance of ordered connected parts.

Fig. 2.18. Charge conjugation relationship for ordered connected parts of self-conjugate particles.

We point out here a confusing facet of charge-conjugation invariance for ordered and planar connected parts. One expects charge-conjugation invariance to require vanishing of connected parts for self-conjugate particles when the product of all symmetry factors is -1. Such vanishing, however, does not occur for ordered connected parts – where charge conjugation produces an inversion of order. The vanishing *does* occur for a planar connected part, because within the superposition by which the latter is constructed (e.g. fig. 2.8 with all plus signs because self-conjugate particles must be bosons) every ordered connected part may be paired with one of opposite order. If the overall product of charge-conjugation symmetry factors is -1, the two members of each pair cancel each other [11, 12].

The consistent factorization of the poles of the planar S matrix ensures that they will respect the charge-conjugation selection rule. In fig. 2.9, for example, if particles A, B, C, D, E are all self conjugate, the pole residue is nonvanishing only if $C_{\mathrm{E}} = C_{\mathrm{A}}C_{\mathrm{B}} = C_{\mathrm{C}}C_{\mathrm{D}}$. Discontinuities of planar connected parts, however, do *not* generally respect charge-conjugation selection rules. For example, the eight-term superposition corresponding to figures 2.13 and 2.14 (again, with all positive signs) does not vanish when $C_{\mathrm{E}}C_{\mathrm{F}} = -C_{\mathrm{A}}C_{\mathrm{B}} = -C_{\mathrm{C}}C_{\mathrm{D}}$, that is, when the intermediate channel has charge-conjugation symmetry opposite to that of the initial and final channels [13]. As discussed in section 12 it is necessary to include nonplanar terms such as that of fig. 2.15a in order to achieve the expected cancellation.

Exchange degeneracy

We have remarked on the absence of poles and normal thresholds in an ordered connected part from any channel invariant that does not correspond to a cluster of *adjacent* particles in the cyclic order. Within the 4-line ordered connected part of fig. 2.4, for example, if $s_{ij} \equiv (p_i + p_j)^2$, we have poles and normal thresholds in $s_{AB} = s_{CD}$ and in $s_{AD} = s_{BC}$ but not in $s_{AC} = s_{BD}$. Designating the three Mandelstam variables here as $s = s_{AB} = s_{CD}$, $t = s_{AD} = s_{BC}$ and $u = s_{AC} = s_{BD}$, the absence of u singularities means that both in $z_s \equiv \cos\theta_s^{\text{c.m.}}$ and $z_t = \cos\theta_t^{\text{c.m.}}$ there is no "left-hand cut". The Froissart–Gribov partial-wave amplitudes for both s and t ordered reactions then have the property, called "exchange degeneracy", that ordered amplitudes of opposite signature are equal. (Signature need never be introduced.) Regge trajectories for ordered connected parts correspondingly carry no signature label.

Although ordered Regge poles have neither well-defined signature nor well-defined parity, the *product* of signature and parity or "naturality" is meaningful. A similar statement applies to charge-conjugation symmetry for ordered Regge trajectories containing selfconjugate planar particles. The *product* of signature and charge-conjugation symmetry is well defined [10]. Moving along an ordered trajectory planar particles alternate in signature, parity and charge-conjugation symmetry.

When connected parts for the six different orders are superposed to form a four-line planar connected part (fig. 2.8), u singularities will generally occur and exchange degeneracy will be lost. Pole positions cannot, however, be altered by the superposition, so in planar connected parts Regge *trajectories* of opposite signature will continue to coincide. Regge residues of opposite signature are not equal but are simply related [10]. One often characterizes this planar regularity as exchange degeneracy, even though it applies only to Regge poles and not to the full Froissart–Gribov planar amplitude.

Absence of Regge branch points and fixed singularities

The absence of u singularities from the ordered connected part of fig. 2.4 means that the two double discontinuities ρ_{su} and ρ_{tu} both vanish. The usual arguments demanding Regge branch points in J_s and J_t then disappear [5], together with the arguments demanding fixed singularities at nonsense points of unphysical signature. Although no proof has been given,* the absence of Regge branch points and fixed singularities from ordered connected parts has been widely conjectured. Because superposition cannot create new singularities, a similar regularity would attach to planar connected parts. In our review we shall adopt this conjecture and assume the only planar Regge singularities to be moving poles.

3. Internal planar regularities; quark-line diagrams

Any connected part must vanish for combinations of incoming particles that carry a nonzero amount of conserved quantity such as electric charge, but with *ordered* amplitudes there may additionally be a constraint on the allowable order of particles. Ordered connected parts for certain permutations may be required to vanish even though there is a zero net flow of all conserved

* Often invoked is Mandelstam's demonstration that nonplanar Feynman diagrams are needed to generate Regge cuts. Perturbation arguments are inadequate, however, because, as shown in section 8, the ordered S matrix probably has no weak coupling limit.

quantities "into the ring". (An example the reader may anticipate is the vanishing of any ordered amplitude where two planar π^+ particles are adjacent.) The special ordered constraints will turn out to be describable through diagrams that associate planar particles with oriented two-dimensional "strips" whose two opposing edges "carry" the internal quantum numbers. These two edges act in some ways like a quark-antiquark pair, so we shall refer to the pictorial representation of ordered constraints as "quark-line diagrams". Much of the reasoning used in this section is due to Weissmann [7].

It has been shown by Weissmann that if ordered selection rules exist, ordered unitarity requires planar particles to group themselves into distinct families, each family being labeled by a pair of indices (i, j). The first index i labels *another* set of planar particles – those allowed to immediately *precede* (clockwise sense) the (i, j) family members. These predecessor sets are unique and nonoverlapping with each other. The index j labels the set of "successor" planar particles allowed to immediately *follow* the (i, j) family members. Charge conjugation invariance means that for each predecessor set there is a corresponding successor set made up of the antiparticles, so the indices i and j cover the same range. A member of the (i, j) family lies itself in the predecessor set j and at the same time in the successor set i.

We present an outlined derivation of these statements as an example of Weissmann's reasoning. Consider a planar particle A and denote by i_A the set of all planar particles that immediately *precede* A in the counterclockwise permutation of some nonvanishing ordered connected part. According to charge conjugation invariance, the antiparticles of i_A constitute the set of all particles that can immediately *follow* $\bar{A}$. Suppose now that some particle C appears in *both* of two "predecessor" sets i_A and i_B, associated with two *different* particles A and B. There must then exist nonvanishing discontinuity products of the type shown in fig. 3.1 implying that $\bar{B}$ appears

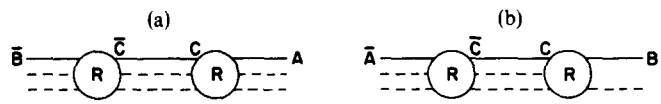

Fig. 3.1. (a) A nonvanishing discontinuity in which C appears as a predecessor to A, and $\bar{C}$ as successor to $\bar{B}$ or, (b) C as predecessor to B, and $\bar{C}$ as successor to $\bar{A}$.

in the predecessor set i_A and $\bar{A}$ in the predecessor set i_B. A similar argument based on fig. 3.2 next allows the conclusion that if any particle *other* than C, say D, appears in i_A it must also appear in i_B. The two sets i_A and i_B must therefore coincide completely if they share *any* particle. Conversely, each planar particle belongs to one and only one predecessor set, which may be designated by an index i that makes no reference to any of the particles for which i is the predecessor set.

The foregoing line of reasoning evidently can be applied also to the set of planar particles immediately *following* (clockwise sense) some designated planar particle, leading to identification of unique and nonoverlapping "successor" sets. We have already remarked how charge conjugation invariance guarantees that for each "predecessor" set i there is a successor set consisting of the corresponding antiparticles. A natural convention is to designate the latter set with the same index i, making explicit that predecessor sets are in one-to-one correspondence with successor sets.

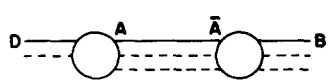

Fig. 3.2. A discontinuity which establishes D as a predecessor to B.

These requirements are compactly summarized by requiring any nonvanishing connected part to be representable through a diagram of the type of fig. 3.3, where the family indices appear on directed "links" connecting successive particles. Particle A belongs to the family (i, j), B to the family (j, k) and so on. For some purposes it is helpful to visualize the succession of directed links in fig. 3.3 as the boundary of a two-dimensional oriented surface. Isolating an individual planar particle, we then associate it with an oriented "strip" whose two edges – corresponding to predecessor and successor links – characterize the (internal) selection rules.

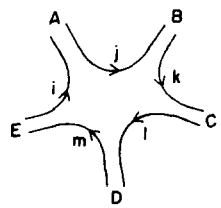

Fig. 3.3. Quark-line diagram for an ordered connected part.

Now consider an additively-conserved internal quantum number Q, such as electric charge. How can conservation of Q be compatible with the rules embodied in fig. 3.3? A natural guess is that all planar particles belonging to a family (i, j) share a common value of Q, a value that we designate as Q_{ij}. (Weissmann has shown that, if such is not the case, then all values of Q from $+\infty$ to $-\infty$ must appear on particles in the planar spectrum.) The requirement that incoming Q's shall sum to zero can then be shown to imply that Q_{ij} depends on the indices i and j according to the rule:

$$Q_{ij} = q_j - q_i. \tag{3.1}$$

Here we see the quark–antiquark role for the two links. The rule (3.1) is equivalent to saying that link i "carries" a charge q_i. The opposite direction of the two links means that a planar particle belonging to a family (i, j) has charge equal to that of a "quark" of type j plus that of an "antiquark" of type i.

We are hoping to establish a correspondence between planar particles and physical particles, so we are led to ask for the minimum number of link types (predecessor or successor sets) capable of accommodating the observed additively-conserved hadronic internal quantum numbers. Putting aside baryon number for the moment, experiment tells us that at least strangeness and charm must be considered in addition to electric charge. With no conserved quantities at all, there would already be one link type, so in order to encompass three conserved quantities we need $3 + 1 = 4$ link types. Table 3.1 shows one straightforward way of attaching quantum numbers to links.

Table 3.1

Link type (successor index)	Charge	Strangeness	Charm
1 n	0	0	0
2 p	1	0	0
3 λ	0	−1	0
4 c	1	0	1

Should further conserved quantities be discovered, one adds more link types. A total of N different links can accommodate $N - 1$ additively-conserved quantum numbers. In the language of flavors, we have one link type for each flavor.

Because the quantum numbers of a planar particle, according to formula (3.1), reflect only the *differences* of the quantum numbers attached to the two associated links, one may add any constant to the latter without changing the ordered S matrix. In particular we may uniformly subtract 1/3 from each entry in column 1 of table 3.1 so as to achieve the usually-assigned fractional quark charges. (When baryons are incorporated into an ordered S matrix the link quantum numbers will become unambiguous.)

We emphasize that the planar family assignments in table 3.1 are tentative and subject to self-consistency checks with respect to ordered discontinuity formulas. Weissmann's reasoning permits an arbitrary collection of link types but this reasoning has only considered the topological constraints of ordered discontinuity formulas – not the dynamical constraints flowing from the character of the latter as nonlinear relations between ordered amplitudes. It may be hoped that the existence of a variety of flavors is uniquely required by ordered unitarity.

Why have we not included baryon number in table 3.1? It will be seen in section 13 that a more complex notion of particle ordering than a simple linearly-linked chain is needed in order to describe baryons. The connection with the quark concept reached in the present section shows that simple sequential ordering, together with ordered selection rules, implies $q\bar{q}$ structure but not qqq. Section 13 describes a generalization of the notion of particle order that maintains the essential characteristics of planarity and that yields a planar spectrum corresponding to qqq and $\bar{q}\bar{q}\bar{q}$, with certain superpositions and contractions thereof. The more general ordered S matrix may be split into noncommunicating sectors* one of which, containing only $q\bar{q}$ states with baryon number zero, is closely related to the simple sequentially-ordered S matrix; all external and internal regularities remain the same. The considerations of the present section will survive the generalization but they apply only to "ordinary" mesons.

The assignment in table 3.1, together with fig. 3.3, leads to a collection of remarkable "internal" planar regularities for mesons. In addition to the requirement that planar mesons fall into families with $q\bar{q}$ quantum numbers (no "exotics"), the demand that the succession of links constitute a single boundary leads to the OZI rule forbidding any reaction not depictable in the connected form of fig. 3.3. Consider for example the four-particle reaction

$$A(n, p) + B(p, n) \to \overline{C(\lambda, c)} + \overline{D(c, \lambda)}.$$

Although all internal quantum numbers are conserved, there is no connected quark-line diagram, so the reaction is forbidden at the planar level. Representation of this reaction requires two disconnected boundaries, and the reaction becomes allowed only at a higher level of the topological expansion (see section 11).

An important special case of the OZI rule relates to planar particles of the type (i, i), which carry overall zero quantum numbers but which have no planar communication with channels where the link type i fails to appear, even though the overall channel quantum numbers are zero. Section 4 will discuss the relevance of the OZI rule to the stability of (c, c) (charmonium) and (λ, λ) (strange-

* Although the different sectors do not communicate through ordered unitarity, a *complete* understanding of any one ordered sector involves all the others.

onium) states like ψ, ψ', φ and f'. The physical consequence for the (n, n) and (p, p) families is more tricky because of isospin symmetry, which means that every (n, n) planar particle has a degenerate (p, p) partner. As always the case with degenerate quantum systems, one then finds it physically useful to consider those special linear superpositions that are unmixed by elements of the symmetry group. In the present case the two superpositions are the symmetric and antisymmetric combinations $[(n, n) \pm (p, p)]/\sqrt{2}$, corresponding to $I = 0,1$ with $I_z = 0$. With such states the usual OZI rule becomes replaced by a statement of *degeneracy* between $I = 0$ and $I = 1$ in the ordered S matrix. Section 4 considers the experimental evidence for such degeneracy. Notice that we have given no argument *requiring* internal symmetry (such as isospin invariance) in the ordered S matrix. Such arguments may eventually emerge from nonlinear unitarity (dynamical) requirements.

Were SU_3 symmetry exact (or almost exact), physical expression of the OZI rule would be a prediction of symmetry between octets and singlets rather than a rule forbidding certain decays of (λ, λ) states. To decide whether the internal planar regularity is more usefully described as an OZI selection rule or as an SU_N multiplet degeneracy, the important question is whether the breaking of SU_N symmetry is large or small compared to the departure from planarity of the physical particles in question. SU_2 symmetry breaking is so small that here one chooses to emphasize isospin degeneracy, whereas SU_3 and SU_4 symmetry breaking is so large that one usually (although not always) chooses to think of an OZI selection rule. Sections 10 and 11 discuss these subtle issues; a superficial discussion unavoidably occurs already in section 4.

4. How planar is the physical S matrix?

The planar S matrix plays a central role in the topological expansion – serving as the starting point. It is correspondingly important to known how closely the physical S matrix resembles its planar counterpart; it would be reassuring to establish that the planar S matrix gives a reasonably accurate representation of the real world. In order to discuss baryons we shall need a generalization of the simple sequential ordering on which the planar S matrix is based, but for the meson sector of $q\bar{q}$ states the external regularities described in section 2 and the internal regularities described in section 3 will survive the generalization. Let us consider first the extent to which observed mesons exhibit the characteristic external planar regularities required by ordered unitarity.

Exchange degeneracy of Regge trajectories

At the heart of planarity is the absence of certain discontinuities from ordered connected parts. We have stressed in section 2 the consequence that Regge trajectories of the planar S matrix occur in degenerate pairs of opposite signature – a property known as exchange degeneracy (EXD). To what extent do physical meson trajectories display EXD?

The leading (highest angular momentum at fixed mass) hadron trajectories contain mesons of natural parity and "natural charge conjugation symmetry". The tendency of this entire group of trajectories to occur in EXD pairs is striking. The odd-signature, zero-strangeness $I = 1$ trajectory, containing the ρ $(J = 1)$ and g $(J = 3)$ mesons, has been experimentally determined over the interval $-1\ \text{GeV}^2 \lesssim t \lesssim 3\ \text{GeV}^2$. The corresponding even-signature trajectory, containing the A_2 $(J = 2)$ meson, has been determined over a comparable interval and, as shown in fig. 4.1, is found to deviate from the odd-signature trajectory by no more than ~ 0.1 units in J. The deviation near $J = 2$ is in fact much less. The accuracy with which the A_2 trajectory coincides with the ρ

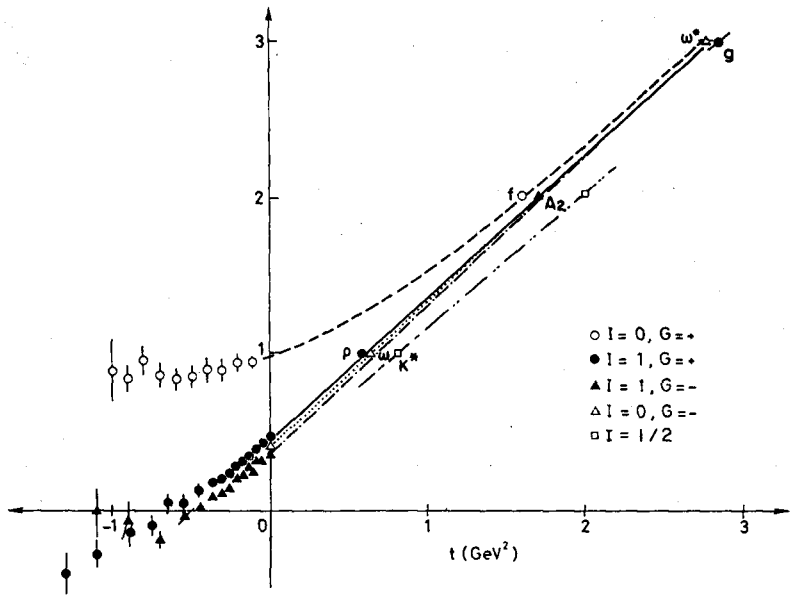

Fig. 4.1. The observed Regge trajectories for the leading families of mesons. The various lines are not fits, but are meant to guide the eye. For $t > 0$ EXD is seen to be very good. We have assumed pomeron-f identity (see section 10).

trajectory is far better than the accuracy of SU_3 symmetry, approaching the accuracy of SU_2 symmetry. For the leading $I = 0$ (nonstrange) trajectories EXD is experimentally well satisfied for $t \gtrsim 0.5$ GeV^2 although for $t \lesssim 0$ there is an important degeneracy breaking associated with the concept of pomeron. We shall deal in detail with the latter phenomenon in section 10, where we show that a large deviation from planarity in the $I = 0$ low-t sector is to be expected. No such large deviation is expected in the $I = 1/2$ sector and, indeed as seen in fig. 4.1, the K* ($J = 1$) and K** ($J = 2$) trajectories display a degree of EXD comparable to that of ρ and A_2. In section 12 we shall see how even the small $I = 1/2, 1$ deviations from EXD may be systematically and quantitatively explained through a nonplanar component of the topological expansion.

For the next group of meson trajectories – which have unnatural parity – there is less experimental knowledge but the general pattern appears similar. Except for $I = 0$ at low t the data is compatible with reasonably-accurate EXD: for example, exchange-degeneracy between the π and B trajectories. Thus within the meson sector there is general adherence to exchange degeneracy – with the important $I = 0$, low-t exceptions, to which we intend to give extensive attention.

Weakness of Regge cuts; short-range order in rapidity

Less striking than EXD but still worthy of note is the apparent weakness of Regge cuts in observed physical amplitudes. In section 2 we drew attention to the widespread belief that the only Regge singularities of the planar S matrix are factorizable (moving) poles. A qualitatively-remarkable aspect of high-energy hadron reaction experiments is the extent to which a simple Regge-pole description has turned out to be successful both for exclusive and inclusive measurements. The concept of short-range order in rapidity has been of great phenomenological utility; such short-range order – a consequence of factorizable Regge poles – is not easily understood if Regge cuts are important. The general success of Regge-pole representations is so well established that one

easily forgets the need to understand why other Regge singularities are less significant. If we are able to explain why nonplanar components of the topological expansion are small, we expect automatically to understand why Regge cuts are weak.

Isospin degeneracy

Passing to internal planar regularities, let us consider the property of $I = 0$, 1 degeneracy – predicting quartets of equivalent nonstrange, noncharmed states. In the physical S matrix the (ρ, ω) and (A_2, f) combinations provide outstanding examples with respect to both masses and couplings. The observed deviations from degeneracy are strikingly small. When the concept of isospin degeneracy is extended to Regge trajectories we find, just as for $I = 0$ exchange degeneracy, that deviations become large at small t. The explanation, discussed in section 10, is closely related to that for low-t EXD breaking.

The lowest-mass unnatural-parity mesons, π and η, seem to display a large deviation from isospin degeneracy, but the breaking is no larger than expected for such low-mass states from the nonplanar components of the topological expansion needed to restore unitarity. The degree of $\pi - \eta$ isospin-degeneracy breaking is similar in magnitude to the EXD breaking responsible for pomeron phenomena.

OZI selection rule

Section 3 drew attention to certain reactions forbidden at the planar level because of not corresponding to single-boundary (connected) quark-line diagrams [14]. To consider experimental evidence on such reactions we need to associate physical particles with planar families. Within the group of leading physical mesons the following association follows straightforwardly on the basis of quantum numbers:

Family	$J^{PC} = 0^{-+}$	1^{--}	2^{++}
n, p	π^+	ρ^+	A_2^+
λ, n	K^0	K^{0*}	K^{0**}
λ, p	K^+	K^{+*}	K^{+**}

Isospin degeneracy allows the further identifications,

$[n, n + p, p]/\sqrt{2}$	η	ω	f
$[n, n - p, p]/\sqrt{2}$	π^0	ρ^0	A_2^0

although as noted above the physical η is badly split from the π. When antiparticles are considered we have accounted in the above listing for 8 of the 9 planar families associated with the first three flavors (isospin and strangeness). What physical particles should be associated with the remaining (λ, λ) family? To the extent that SU_3 nonet groupings are experimentally recognizable, it is natural to assign the ninth member to this final category:

λ, λ $\quad \eta' \quad \varphi \quad f'$.

With this complete set of assignments we are in position to discuss the experimental status of the OZI rule [14].

The most celebrated examples of OZI-forbidden reactions are decays of the type

$$(\lambda, \lambda) \to (\mathrm{p}, \mathrm{n}) + (\mathrm{n}, \mathrm{p})$$

which conserve all internal quantum numbers but which do not admit a connected quark-line diagram. Illustrations are $\varphi \to \pi^+\rho^-$ and $\mathrm{f}' \to \pi^+\pi^-$. When compared to the corresponding decays $\omega \to \pi^+\rho^-$ and $\mathrm{f} \to \pi^+\pi^-$ – allowed by the OZI rule – a dramatic suppression has been experimentally found. The available evidence, recently compiled by Okubo [15] indicates a high degree of planarity in this sector of the physical S matrix. We shall see, furthermore, in section 11 that the small observed rates of these OZI-forbidden decays are understandable through unitarity-required corrections to the planar S matrix. All 2-particle decays of η and η' are forbidden by standard selection rules, so no similar experimental tests of the OZI rule are possible here.

Also reviewed by Okubo is evidence that φ and f' are produced much less frequently than ω and f in reactions where the other particles do not "contain" strange quarks. These reactions involve baryons and cannot be systematically considered until a generalization has been made of the planar S matrix. It is natural, however, to anticipate some form of connected quark-line representation and a generalized OZI rule, with planar baryons classified into (i, j, k) families (a baryon "without strange quarks" is one belonging to a planar family where neither i nor j nor k is a λ). Reactions involving baryons may then be admitted into evidence and, as shown by Okubo [15], they give impressive additional support to planarity as a good physical approximation. We remark that, even when initial particles contain no strange quarks, production of φ and f' may be allowed on a planar level if other "strangeness-carrying" particles like K or K* are produced. As discussed by Okubo [15], it is found experimentally that reactions involving η' and η display less planarity than those involving φ, ω or f' and f. The degree of nonplanarity is, however, no greater than already indicated by the $\pi - \eta$ mass splitting. Section 10 will show that all these $I = 0$ deviations from simple planar behavior are understandable through the second term of the topological expansion – the leading correction required by unitarity.

The reader need hardly be reminded of the spectacular accuracy of the OZI rule for charmonium (c, c) states. Again we refer to the Okubo review [15] for details. In section 11 we explain why mesons of increasing mass are expected to show increasingly accurate planarity.

To summarize this section, there exists widespread evidence that the meson sector of the physical S matrix is approximately planar. It is then reasonable to treat corrections to the planar S matrix by perturbation techniques and, except for sections 9 and 13, the remainder of our review is devoted to such corrections.

5. The S-matrix topological expansion

It was emphasized in section 2 that the extreme degree of order embodied in the planar S matrix is inconsistent with unitarity. The present section will show how one attempts systematically to regain unitarity through a succession of corrections to the planar S matrix. Since the succession is constructed through topological considerations we begin by reviewing some properties of graphs with *ordered* vertices. Physically the reader may anticipate that such vertices are to be associated with the ordered connected parts defined in section 2.

Graphs with ordered vertices

By an ordered vertex we mean one whose attached lines lie in a definite cyclic sequence – admitting the two-dimensional graphical representation illustrated in fig. 5.1. Here we show a 5-line vertex with the cyclic order BEADC as well as a four-line vertex with the order FGDC. (A convention must be adopted to associate the stated order of lines with a sense of rotation about the vertex – clockwise or counterclockwise. We have chosen the clockwise sense in fig. 5.1, consistent with sections 2 and 3, and will continue this convention throughout our review.) We have seen already in section 2 how the unitarity condition on the S matrix, which involves products of connected parts, leads to consideration of "products of ordered vertices" where certain lines from one vertex are identified (joined) with certain lines from another vertex (figs. 2.14 and 2.15). Suppose in fig. 5.1, for example, that the initial channel contains two particles corresponding to lines F and G while the final channel contains three particles corresponding to the lines A, B and E. Suppose further that a channel communicating with both of the foregoing channels contains two particles corresponding to the lines C and D. Unitarity will then lead us to consider the product graph corresponding to the dotted lines in fig. 5.1 joining the two vertices.

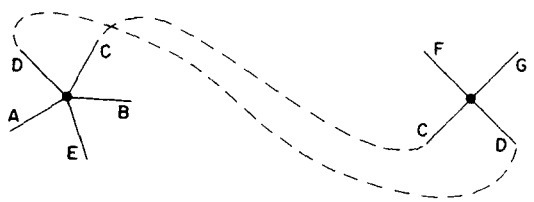

Fig. 5.1. A five line vertex BEADC, a four line vertex FGDC, and their connection (dotted line) in a unitarity product.

More generally, if unitarity is used to prescribe iterative corrections to a starting approximation based on ordered amplitudes, one anticipates a characterization of S-matrix components through the topology of graphs built from ordered vertices.

Boundaries and handles as expansion parameters

It is known that each graph built from ordered vertices may be mapped (without crossing of lines) onto a two-dimensional surface of uniquely prescribable "minimal topological complexity". The surface is characterized by the number of "handles" h and by the way in which external lines are attached to various boundaries. We show below, with examples, how the classification of an arbitrary graph is achieved. Let us tentatively assume, subject to the requirement of consistency with unitarity, that a physical connected part describing the interaction of particles A, B, C, ... may be decomposed into a series of components each belonging to a definite two-dimensional topology. Following Veneziano [3, 16], we call this decomposition the "topological expansion":

$$M^{A,B,C\ldots} = \sum_{h=0}^{\infty} \sum_{b_1,b_2\ldots} M_h^{b_1,b_2,\ldots}. \tag{5.1}$$

A boundary b_i accommodates a subset of the external lines in a definite cyclic order, so the possible values taken by boundary indices are enumerable by dividing the total number of external lines into all possible subsets and within each subset considering all possible cyclic orderings. To avoid

misunderstanding let us write out the explicit boundary structure in the topological expansion of a 4-line connected part:*

$$M^{A,B,C,D} = \sum_{h=0}^{\infty} M_h^{ABCD} + M_h^{ABDC} + M_h^{ACBD} + M_h^{ADBC} + M_h^{ACDB} + M_h^{ADCB}$$
$$+ M_h^{AB,CD} + M_h^{AC,BD} + M_h^{AD,BC}$$
$$+ M_h^{A,BCD} + M_h^{A,DCB} + M_h^{B,ACD} + M_h^{B,DCA} + M_h^{C,ABD} + M_h^{C,DBA} + M_h^{D,ABC} + M_h^{D,CBA}$$
$$+ M_h^{A,B,CD} + M_h^{A,C,BD} + M_h{}^{AB,C,D} + M_h^{A,D,BC} + M_h^{AC,B,D} + M_h^{AD,B,C} + M_h^{A,B,C,D}. \quad (5.2)$$

The order in which the different boundaries are listed is meaningless and cyclic permutations of lines on a given boundary leave the topology unaltered. For example,

$$M_h^{A,BCD} = M_h^{BCD,A} = M_h^{CDB,A}.$$

It is evident that the total number of boundaries cannot exceed the total number of external lines. The reader will no doubt have surmised that the components with a single boundary and no handles comprise what we have in section 2 called the planar S matrix. Later in the present section we shall return to this important physical point, but first we deal with some purely mathematical questions.

How does one determine the topological classification of a graph built from ordered vertices? We state here a prescription given by Edmonds [17], drawn to our attention by Stapp. Take any graph, such as the 4-vertex, 6-external line example of fig. 5.2. We assume that all internal lines

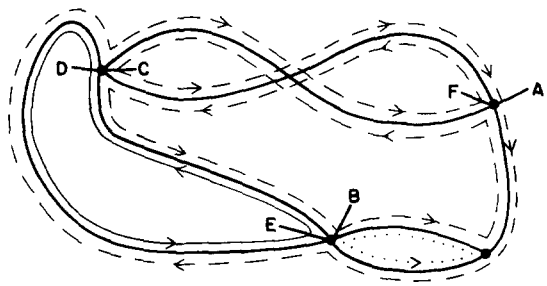

Fig. 5.2. A graph with 4 vertices, 6 external lines, and 7 internal lines (dark lines). The thin line, dotted line and dashed line are orbit paths.

connect different vertices. Edmonds' rule avoids the need to construct explicitly the two-dimensional surface on which the graph is to be mapped. Working directly with the graph, start at any external line and proceed clockwise around the vertex until reaching the first line that is not external. Then follow that line to the next vertex, at which point the process is repeated – always proceeding clockwise around each vertex. Eventually one will return to the starting point. The complete closed orbit defines a boundary. All external lines that have been crossed in such an orbit may be said to exit from the same boundary and in a definite (cyclic) order. In fig. 5.2, for example, the lines A, F, B and C, in that order escape from the dashed boundary, while the lines D and E escape from the thin boundary. Readers conditioned to quark-line diagrams may feel the urge to associate quarks with Edmonds' "orbit" connecting points on the same boundary,

* The internal quantum number selection rules of section 3 may require certain components to vanish.

but Edmonds presumably had never heard of quarks when he devised this solution to a purely topological problem.

For a given graph let us introduce a parameter $b_{\max}$ giving the total number of different boundaries that would occur if at least one *additional* external line were inserted between any adjacent pair of internal lines at each vertex. More concisely, $b_{\max}$ is the total number of different orbits that can be traced through the graph by Edmonds' rule regardless of whether the orbit crosses an external line.* In the graph of fig. 5.2, $b_{\max} = 3$. The parameter $b_{\max}$ is important because of a formula due to Euler that determines the (minimum) number of handles on the embedding two-dimensional surface. If the total number of vertices is v and the total number of internal lines is e (in fig. 5.2, $v = 4$ and $e = 7$), then Euler's formula for the minimum number of handles is

$$h = \frac{2 + e - v - b_{\max}}{2}. \tag{5.3}$$

Using Euler's rule we find that the minimum number of handles, on a two-dimensional surface capable of accommodating the graph of fig. 5.2, is $h = 1$. (Such a surface is often called a torus.) A connected-part component with the topology of fig. 5.2 we designate in the notation of eq. (5.1) by $M_1^{\mathrm{AFBC,DE}}$. The reader may verify that a connected-part component with the topology of fig. 5.1 would be designated by $M_0^{\mathrm{FG,BEA}}$.

Graph representations of connected-part components

A graph consisting of a single vertex (no internal lines) may be mapped onto a surface with no handles and a single boundary. A connected-part component with such topology is of the class $M_0^{\mathrm{ABC}\cdots}$ – often characterized as the planar class. Conversely we may associate any component in this especially simple class with a single vertex. Also lying in the planar class are equivalent 2-vertex graphs of the type illustrated in fig. 5.3, it being convenient to use a 2-vertex representation when discussing poles and discontinuities. (We shall rarely need to go beyond 2-vertex representations.) The topological equivalence of different graphs implies their physical equivalence – a manifestation of duality.

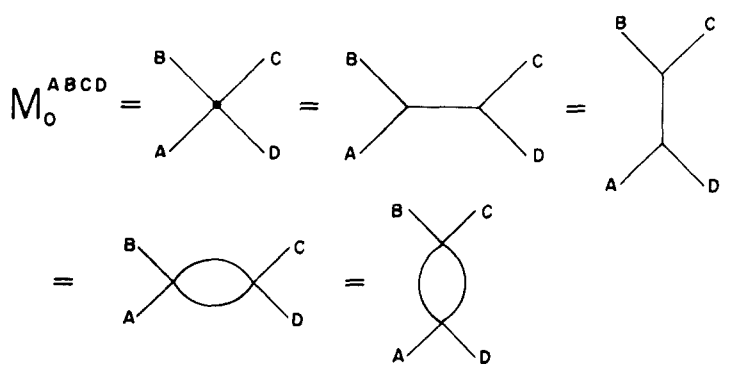

Fig. 5.3. Equivalent 1 and 2 vertex graphs which are members of the same planar class.

* All possible orbits will have been enumerated when each internal line is seen to have orbits on both sides. The directions of these two orbits are necessarily opposite.

With the constraint that internal lines must not begin and end at the same vertex, representation of connected-part components with $h = 0$ but more than one boundary requires at least two vertices. Consider components with no handles but two boundaries – often called "cylinders". Figure 5.4 shows several equivalent 2-vertex representations of a cylinder component. Different

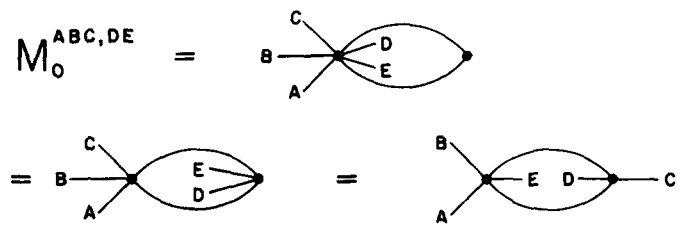

Fig. 5.4. Equivalent 2-vertex representations of a cylinder component.

graphical representations are useful in connection with different discontinuities. In fig. 5.5 we show possible 2-vertex representations of a zero-handle component with 3 boundaries. When

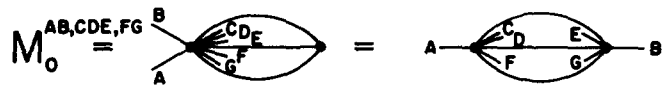

Fig. 5.5. A possible 2-vertex representation of a zero-handle component with 3 boundaries.

handles are present we can still find 2-vertex representations, such as shown in fig. 5.6 for a 1-handle, 1-boundary example. Although all topological information resides in the notation $M_h^{b_1,b_2\cdots}$ we shall nevertheless often find it helpful when considering discontinuities to employ explicit graphical representations.

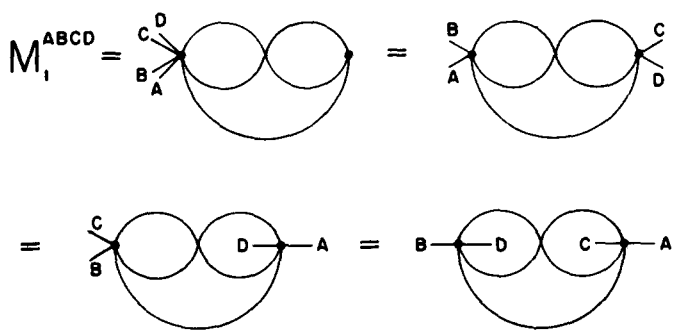

Fig. 5.6. Possible 2-vertex representations for a 1-handle, 1-boundary component.

Unitarity

The S-matrix topological expansion is physically useful because it dovetails with the structure of the unitarity condition. Suppose that we wish to calculate a two-particle discontinuity in the

AB → CD channel invariant of a four-line connected part, arising from an intermediate channel EF. The general formula has the structure

$$\mathrm{disc}_{\mathrm{AB(EF)}} M^{\mathrm{A,B,C,D}} = M^{\mathrm{C,D,E,F}} \otimes M^{\mathrm{E,F,A,B}}. \tag{5.4}$$

Let us substitute an expansion of the form (5.2) into both sides of (5.4). By using graphical representations of the kind shown in figs. 5.3–6, together with Edmonds' rule, it is straightforward to identify the topology of any individual product term and to collect terms of common topology. We find first of all

$$\mathrm{disc}_{\mathrm{AB(EF)}} M_0^{\mathrm{ABCD}} = M_0^{\mathrm{CDFE}} \otimes M_0^{\mathrm{EFAB}} + M_0^{\mathrm{CDEF}} \otimes M_0^{\mathrm{FEAB}}, \tag{5.5}$$

corresponding to fig. 5.7, with similar formulas for the discontinuity of M_0^{ABDC}, M_0^{ACDB} and M_0^{ADCB}.

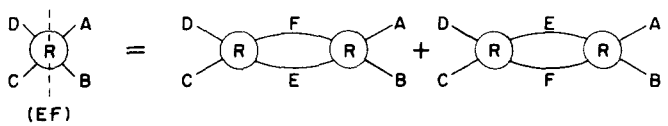

Fig. 5.7. Graphical representation of eq. (5.5), for ordered unitarity.

At the same time the discontinuity of M_0^{ACBD} and M_0^{ADBC} is found to vanish. We have here precisely the discontinuity prescription for an ordered connected part discussed in section 2, a correspondence that can easily be extended to an arbitrary discontinuity of an arbitrary ordered connected part. Assuming amplitudes to be determined by their singularities, we may now therefore consistently make the postulate that: *the single-boundary zero-handle components of the topological expansion are the connected parts of the ordered S matrix.* In making this postulate we implicitly adopt as the basis for our Hilbert space the poles of the ordered S matrix, i.e. the planar particles. These particle-poles constitute a suitable basis because the unitarity of the ordered S matrix guarantees their factorizability.

Passing to the discontinuity of cylinder components with $h = 0, b = 2$ we find product members with $h = 0$ but $b = 1$ as well as $b = 2$:

$$\mathrm{disc}_{\mathrm{AB(EF)}} M_0^{\mathrm{AC,BD}} = M_0^{\mathrm{CEDF}} \otimes M_0^{\mathrm{FBEA}} + M_0^{\mathrm{CFDE}} \otimes M_0^{\mathrm{EBFA}}, \tag{5.6}$$

$$\begin{aligned}\mathrm{disc}_{\mathrm{AB(EF)}} M_0^{\mathrm{ABC,D}} = {} & M_0^{\mathrm{CEDF}} \otimes M_0^{\mathrm{EABF}} + M_0^{\mathrm{CFDE}} \otimes M_0^{\mathrm{FABE}} + M_0^{\mathrm{D,CEF}} \otimes M_0^{\mathrm{FEAB}} \\ & + M_0^{\mathrm{D,CFE}} \otimes M_0^{\mathrm{EFAB}},\end{aligned} \tag{5.7}$$

$$\begin{aligned}\mathrm{disc}_{\mathrm{AB(EF)}} M_0^{\mathrm{CD,AB}} = {} & (M_0^{\mathrm{DCFE}} + M_0^{\mathrm{CDFE}}) \otimes (M_0^{\mathrm{FEAB}} + M_0^{\mathrm{FEBA}}) \\ & + (M_0^{\mathrm{DCEF}} + M_0^{\mathrm{CDEF}}) \otimes (M_0^{\mathrm{EFAB}} + M_0^{\mathrm{EFBA}}) \\ & + (M_0^{\mathrm{CDFE}} + M_0^{\mathrm{DCFE}} + M_0^{\mathrm{CDEF}} + M_0^{\mathrm{DCEF}}) \otimes M_0^{\mathrm{EF,AB}} \\ & + M_0^{\mathrm{CD,EF}} \otimes (M_0^{\mathrm{EFAB}} + M_0^{\mathrm{EFBA}} + M_0^{\mathrm{FEAB}} + M_0^{\mathrm{FEBA}}) + M_0^{\mathrm{CD,EF}} \otimes M_0^{\mathrm{EF,AB}}\end{aligned} \tag{5.8}$$

with analogous formulas for other orderings. These examples exhibit the kind of unambiguous discontinuity formula that exists for each component of the topological expansion. These are the

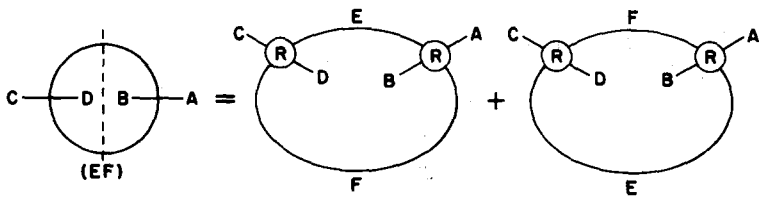

Fig. 5.8. Graphical representation of the cylinder discontinuity eq. (5.6).

DTU dynamical equations, from which all quantitative predictions flow. In subsequent sections we shall return to the above cylinder formulas, which have important physical implications.*

We do not attempt an exhaustive catalogue of properties for topological discontinuity formulas but point out that the number of handles in any product cannot be less than the sum of the number of handles in the two product members. Thus the discontinuity formula for a component with h handles only involves components with handle number less than or equal to h. We have seen an important special case of this rule in the above $h = 0$ illustrations. Another simple rule is that adjacent particles on a single boundary of a product member cannot appear on different boundaries of the product. Inspection of our $h = 0$ sample formulas will verify this rule. We mention finally that if a product is to have fewer boundaries than the product member with the larger boundary number, additional handles must be created. We recognize in such rules a kind of conservation law for degree of complexity which will allow us systematically to build up disorder starting from the maximal order of the planar S matrix. Increasing degree of disorder is measured by a combination of the number of handles and the number of boundaries.**

Convergence

The usefulness of the topological expansion (5.1) depends on its rate of convergence, which is believed to be rapid in certain important sectors of the S matrix. Section 4 has reviewed experimental evidence suggesting that the components with zero handles and one boundary constitute a good approximation in the meson sector. These experimental indications, together with internal quantum-number convergence arguments that will be reviewed in section 7, encouraged Veneziano in arriving at his proposal. Later there developed awareness [19] of a dynamical mechanism tending to suppress components of higher complexity, that is related to the peripheral character of strong interactions. The mechanism, to be discussed in the following section, may be described as "peripheral suppression of nonplanarity"; it stems from the absence of certain singularities from ordered amplitudes.

6. Peripheral suppression of nonplanarity

In this section we show how the peripheral character of strong interactions tends to suppress the importance of nonplanar components within the topological expansion. We begin by expressing the notion of peripheralism through the concept of "strips" in the space of channel invariants.

* The intermediate particles E and F may be replaced by ordered clusters of particles to obtain the general cylinder discontinuities.

** Sursock [18] has shown that the number of handles and boundaries associated with a product of two ordered amplitudes is determined by the transpositions needed to bring the two orders into correspondence.

Strip structure of connected parts

A peripheral amplitude has the property of being small except in strips that run parallel to the asymptotic boundaries of physical regions, that is, parallel to the lines $s_i = 0$. Although never mathematically proved, peripheralism is believed to be a consequence of Regge behavior. With respect to a 4-line connected part the origin of peripheralism is seen in the following considerations: Decompose the connected part into two portions corresponding to right- and left-hand cuts in some z_i – the cosine of the scattering angle in one of the reactions described by the connected part. Make an appropriate partial wave analysis of each portion,

$$F^{\mathrm{L,R}} = \sum_J (2J + 1) P_J(z_s) F_J^{\mathrm{L,R}}(s)$$

and express the partial waves through Froissart–Gribov formulas in terms of discontinuities in z_i and second-kind representation functions of the rotation group [4, 5]

$$F_J^{\mathrm{L,R}}(s) = \frac{1}{\pi} \int_1^\infty \mathrm{d}z D^{\mathrm{L,R}}(s, z) Q_J(z).$$

The dependence of the partial-wave amplitudes (both magnitude and phase) on angular momentum is then seen to be smooth, with exponential decrease at large J controlled by the z_i singularities nearest to the physical region.

Because the first-kind representation functions (e.g., $P_J(z_i)$) in the ordinary Legendre expansion are all positive and maximum at $z_i = 1$, the "right-hand" (R) amplitude tends there to have a maximum. The "left-hand" (L) amplitude has a maximum at $z_i = -1$. As the scattering angle increases, the representation functions become more and more incoherent and the superposition of partial waves decreases. The angular rate of decrease is greater the larger is the range of important J, the region of large values of the right-hand amplitude being confined within an interval of fixed width in s_i, the channel invariant proportional to $1 - z_i$. A corresponding property holds for the left-hand amplitude. Regge behavior is important to ensure that all partial waves, even the lowest one ($J = 0$ or $1/2$) are part of a single smooth trend. Otherwise cancellation through incoherence of the representation functions will not be fully effective.

The conclusion is that a physical four-line connected part is large only within 3 strips on the Mandelstam diagram, as shown in fig. 6.1.* Such peripheral behavior – so familiar experimentally as to be taken for granted – is highly nontrivial from a theoretical standpoint. Since the underlying basis seems to apply separately to each component of the topological expansion, we shall assume that each component is large only within certain strips.

Generalization of the strip concept to connected parts with more than 4-external particles is tricky because of kinematic constraints on the invariants. A possible resolution of the kinematic problem is reached through Toller variables, each set of which is associated with a tree graph. Thus, for a 5-line connected part we have distinct sets of Toller variables associated with each of the tree graphs of fig. 6.2. Each set contains a *pair* of invariants, associated with internal stems of the tree, that may be simultaneously small. We define a "generalized strip" as the region where *all* the channel invariants belonging to a particular Toller tree graph are small. In other words we make a one-to-one association between tree graphs and strips. (The tree-graph generalization of the

* Our argument has applied only to physical regions, but analyticity considerations suggest that the strip structure is general.

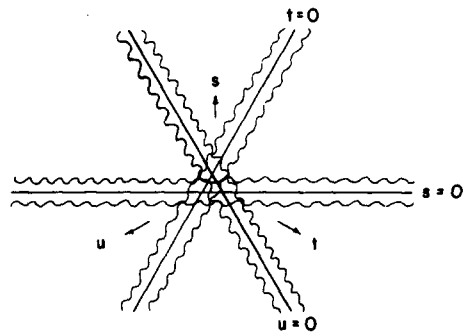

Fig. 6.1. Mandelstam diagram for four-line connected part. Strips where amplitude is large are indicated by wavy lines.

strip concept adapts itself to ordered amplitudes because tree graphs drawn in a plane are automatically ordered.)

Strips in ordered components

Applying the strip concept to a 4-line ordered connected part one finds either a forward or a backward peak in certain channels but not always both. Strips of large amplitude parallel to $s_i = 0$ occur only when s_i is an adjacent-particle channel invariant, i.e. only when there are singularities in s_i.* The strength of the singularities determines the amplitude magnitude within the strips, and for ordered amplitudes there are supposed to be poles as well as branch points in all adjacent-particle invariants. Experience suggests that, when poles are present, amplitudes within strips parallel to the poles are relatively large. We thus expect the ordered amplitude M_0^{ABCD} to be large

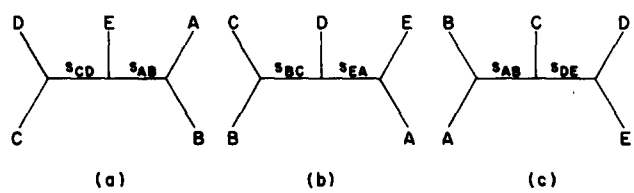

Fig. 6.2. Tree graphs used to define Toller variables.

within the two strips shown in fig. 6.3 and small elsewhere. There is no tendency for M_0^{ABCD} to be large in a strip parallel to $s_{AC} = 0$ because there are no singularities in s_{AC}. When different ordered amplitudes are superposed all three strips will of course be populated.

Poles in nonplanar components

Since all components of the topological expansion are supposed to be determined by their discontinuities, we may infer the singularity structure of nonplanar components from their discontinuity formulas. Now because adjacent particles on a boundary attached to one factor in a

* It is tempting to associate the *nearness* of singularities with the size of the amplitude, but such a notion is treacherous and will be avoided in this paper.

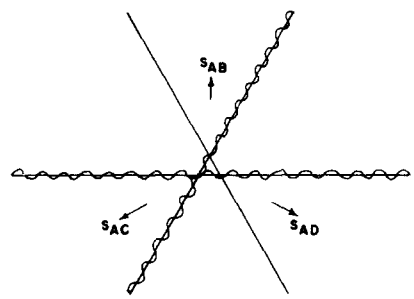

Fig. 6.3. Peripheral strip structure for four-line ordered connected part.

discontinuity product never appear on different boundaries of the product, analysis of the discontinuity formulas reveals something like the Steinmann rule: that poles do not occur in channels containing particles from more than a single boundary. In other words, particles on different boundaries do not resonate with each other.* The point is tricky because channel invariants for particles on different boundaries do have discontinuities, as shown for example by formula (5.6) for a two-boundary cylinder component. Nevertheless, to the extent that planar poles are "transmitted" in a process of iteration starting from single-boundary, zero-handle components (the ordered S matrix), one expects poles to appear only in adjacent-particle invariants.

Strips in nonplanar components

The foregoing pole principle is connected with peripheralism through the assumption that amplitudes are large in peripheral strips *only when poles occur* in conjunction with the associated discontinuity. Our general reasoning about peripheral peaks did not include any statement about the absolute magnitude of a peak. We are now proposing that peripheral peaking is strong only when poles run parallel to the strips. With respect to the strips we have identified for ordered amplitudes, parallel poles are guaranteed to be present, and experience suggests that wherever strong peripheral strips occur, there are parallel poles. Such a statement is equivalent to saying that discontinuities are weak except in the proximity of poles.** So we are led to assume that the important peripheral strips in nonplanar amplitudes correspond to fixed small values for *adjacent-particle* channel invariants.

Let us apply this concept to the two-boundary cylinder component $M_0^{AB,CD}$. We are then led to the strip structure shown in fig. 6.4, the important distinction with the ordered strip structure of fig. 6.3 being that now there is only one strip instead of two. As will be discussed in section 9, at low s_{AB} the cylinder component $M_0^{AB,CD}$ is just as large as a planar component, but the fact that its largeness does not extend over so wide a region will provide a basis for convergence of the topological expansion. In particular, fig. 6.4 will be found immediately to explain the increasing accuracy of the OZI rule with increasing energy.

Readers may wonder why a lengthy discussion of the origin of peripheralism was needed in order to justify fig. 6.4. A simple statement that the only poles of $M_0^{AB,CD}$ are in the variable s_{AB}

* An exception must be made for a boundary containing only one particle or, equivalently, when *all particles* on a boundary are included in the channel whose resonances are under consideration. This exception is related to the cylinder renormalization discussed in section 8 of the special class of particles carrying zero internal quantum numbers. The mechanism discussed in the present section should be understood as applying *after* consistent cylinder renormalization of external particles.

** Section 11 will describe an evaluation of "weak strips" associated with discontinuities in the absence of poles.

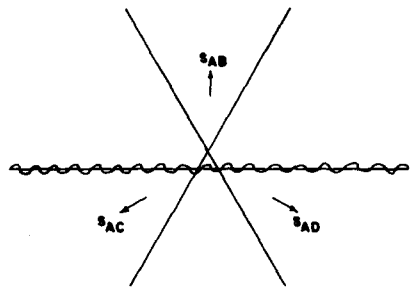

Fig. 6.4. The peripheral strip structure for the cylinder component $M_0^{AB,CD}$.

would not suffice. Such poles might continue to make this amplitude large at large values of s_{AB}. It is angular momentum interference that requires smallness except near the physical boundaries $z_{AC} = 1$ and $z_{AD} = 1$. But peaks at these boundaries we have assumed to be small unless there are poles in s_{AC} and (or) s_{AD}. The only way to resolve such conflicting requirements is for $M_0^{AB,CD}$ to be small over the entire angular range at large s_{AB}.

The more boundaries a component possesses the fewer poles it can have and the smaller the domain over which the component is large. Here is a promising mechanism for convergence of the topological expansion with respect to increasing boundary number. But what about handles? What, for example, is the basis for expecting that the single-boundary component M_1^{ABCD} is small? We here appeal to the notion, explained in section 7, that a handle is like an internal two-boundary cylinder, intermediate particle subchannels flowing into one "boundary" and out the other. The implication of fig. 6.4 is then that only low-mass subchannels are allowed to flow through a handle. There is no constraint on the energy of intermediate subchannels that pass in an ordered fashion on the two-dimensional surface, so the total contribution from ordered intermediate paths tends to be greater than that from handles. Section 12 will elaborate the foregoing mechanism.

7. Internal quantum number suppression of nonplanarity; singlet impotence

Quark-line diagrams have emerged from two different considerations. In section 5 the "orbits" in Edmonds' rule for analyzing nonplanar topological structure were seen to have quarklike appearance, while in section 3 Weissmann's analysis of ordered internal-quantum number selection rules had already, independently, led to quark-line diagrams. What does one learn from diagrams that simultaneously convey information about boundary-handle structure and about internal quantum numbers?

An important observation is that of vanishing net flow of any internal quantum number into an individual boundary; more precisely, quantum numbers must flow into each separate boundary according to the closed-cycle $(i \ldots i)$ pattern of fig. 3.3, for the $A(i, j) \ldots E(m, i)$ connected part. We shall refer to this as the "cylinder flow pattern" since it applies to the quantum number flow through any boundary of a cylinder.

An arbitrary ordered subchannel will not be compatible with such an extremely restrictive pattern. Consider for example a physical A, B, C, D connected part with the family assignments, A(n, p), B(p, λ), C(λ, c), D(c, n). No ordered subchannels here conform to the cylinder flow pattern, so in the topological expansion there can occur only single-boundary components M_h^{ABCD} – com-

ponents with more than one boundary (including cylinders) all vanishing. The foregoing is an extreme example but, in general for a given set of particles A, B ... the larger the number of boundaries the less likely is the possibility of satisfying the cylinder flow pattern.

In the presence of SU_N symmetry a quantitative statement becomes possible. The pattern of fig. 3.3 means that if one forms superpositions corresponding to irreducible representations of the symmetry group, only SU_N *singlet* channels are allowed to flow into an individual boundary [20]. Singlet channels constitute a fraction inversely related to N of all possible ordered channels, so the disfavoring of increasing numbers of boundaries can be related to inverse powers of N. We return below to this question.

It should be emphasized that certain *special* reactions involving singlet subchannels (such as a single $\varphi(\lambda, \lambda)$) receive important contributions from multiboundary expansion components. Confusion exists on this point with respect to the OZI rule. In particular, the statistical mechanism discussed in the present section does *not* explain the stability of strangeonium and charmonium states. As will be seen in section 9, the peripheral mechanism of the preceding section is needed in order to understand these celebrated OZI-rule manifestations.

We next observe that the flow pattern of fig. 3.3 also applies to handles. Consider the single-boundary, single-handle example of fig. 5.6. Compressing the four external lines into a local region of the boundary so as to focus attention on the internal lines that connect the two vertices, the associated quark-line diagram is shown in fig. 7.1 with dotted lines added to identify the handle.

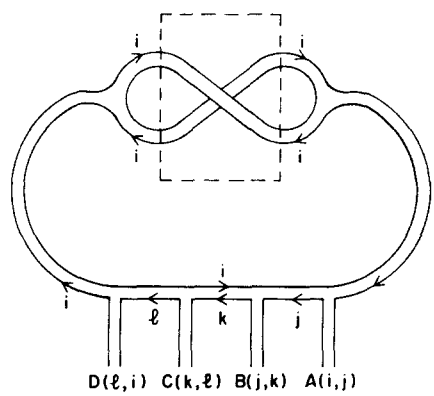

Fig. 7.1. Quark-line diagram for the 1-boundary, 1-handle example of fig. 5.6. Dotted line identifies the quark structure of the handle.

The internal lines flowing into one end of the handle and out the other are seen to exhibit the (i, i) cylinder flow pattern, with the added requirement that the channel flowing into one end is the same as that flowing out the other. Although the representation given by fig. 5.6 of a single-handle, single-boundary component is not unique, any representation must contain a subchannel of intermediate lines exhibiting the cylinder flow pattern. A minimally-required handle may always be visualized as a cylinder that transports a subset of intermediate particles. If the flow pattern is not that of a cylinder the handle is not needed [21].

It was observed by Veneziano that because of the foregoing extreme restriction the number of *intermediate channels*, with a fixed set of (external) boundaries, will systematically decrease as the number of handles increases. Suppose that we think of the topology of fig. 7.1 as arising in a 3-particle AB discontinuity of M_1^{ABCD}, as indicated in fig. 7.2. Compare to the corresponding planar

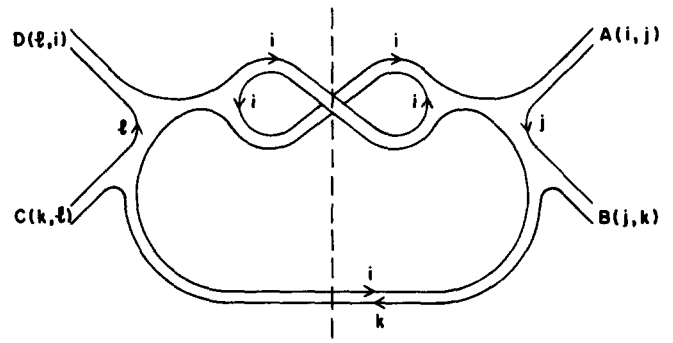

Fig. 7.2. The three-particle contribution to the AB discontinuity of fig. 7.1.

discontinuity of M_0^{ABCD} indicated in fig. 7.3. In the former case the intermediate-particle families $((k,i)(i,i)(i,i))$ are completely determined by the external-particle families $((i,j)(j,k)(k,l)(l,i))$. In the latter (planar) case the intermediate-particle families are less constrained, there being two free boundary indices (n, m). With N different possible values for the boundary index (N different flavors) there are then N^2 different family combinations possible in the planar product's mediate 3-particle channel.

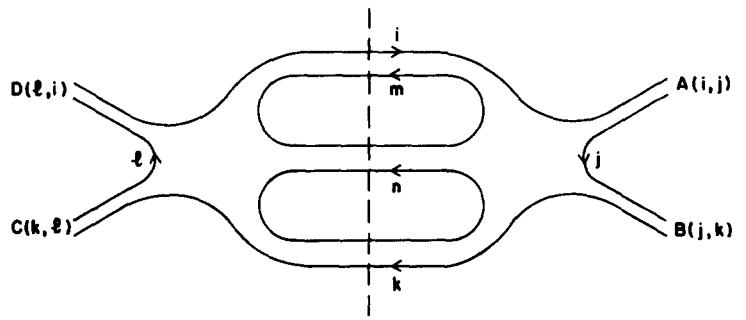

Fig. 7.3. A planar, three-particle contribution to AB discontinuity of an ordered connected part.

Veneziano [3] showed generally that products with the same boundary structure, but a difference Δh in the number of handles, will differ in the number of intermediate channels by a factor $(N^2)^{\Delta h}$. Herein evidently lies a helpful mechanism for convergence of the topological expansion. The mechanism is less effective than the experimental fact, $N \geqslant 4$, might lead one at first sight to suppose because there is kinematical (phase-space) suppression of flavors with high thresholds. Intermediate channels of high threshold, that is to say, are in any case unimportant – even if allowed by topological selection rules. The existence of charm, in particular, does little to improve convergence of the topological expansion. Even strangeness tends to be kinematically suppressed. Isospin symmetry nevertheless guarantees an effective value for N larger than 2, so a respectable role remains for the Veneziano mechanism.*

* Simple models allow one to determine an effective N which is approximately 2.5 when symmetry-breaking is taken into account [13, 22].

Veneziano's result has been qualitatively restated [13] so as to emphasize the connection between boundaries, handles and flavor singlets. When internal symmetry is present we have noted that the S matrix may be diagonalized according to irreducible representations of the symmetry group, only those channels which are singlets with respect to the symmetry group being allowed to pass through (communicate with) an individual boundary. Now we have seen in section 3 that, with SU_N symmetry, planar particles are grouped into multiplets of size N^2. Within such a planar multiplet there is only one singlet state, so the probability that an arbitrary planar particle is permitted to pass (alone) into a boundary is $1/N^2$. This same factor applies also to any multiparticle ordered channel, since the quantum-number structure is similar to that for a single planar particle. Extending the reasoning to intermediate channels or subchannels we see that the probability for an arbitrary channel to be able to pass through a handle is $1/N^2$. Veneziano's mechanism may in this way be ascribed to the statistical impotence of flavor singlets.

We have already warned the reader not to interpret Veneziano's rule as saying that cylinder connections between singlet channels are smaller than planar connections. For reactions involving *external* singlet channels, cylinder components ($h = 0$, $b > 1$) of the S matrix may be just as large as planar components ($h = 0$, $b = 1$). Veneziano's mechanism rests on the relative scarcity of *internal* singlet channels – channels that may pass through handles.

The existence of at least two different convergence mechanisms for the topological expansion renders extremely difficult any general analysis of convergence. Additionally, from the bootstrap point of view (see the end of section 9) one hopes that eventually N (or, more precisely, the distribution of flavor thresholds) will be determined by ordered unitarity, so N is not necessarily a free parameter in the DTU approach.

8. Renormalization of planar poles; cylinder unitarity

The Hilbert space underlying the S-matrix topological expansion is based on the planar particles. Although the planar spectrum is not specified a priori, supposedly being determined through ordered unitarity (i.e. the "ordered bootstrap"; see section 9), planar poles constitute the fabric from which the topological expansion is constructed. Actual poles of the physical S matrix – the sum of all components in the topological expansion – will nevertheless not coincide with planar poles. Such a slippery situation becomes manageable if we remember that full physical unitarity guarantees a consistent factorization pattern for physical poles, just as ordered unitarity guarantees a consistent factorization pattern for planar poles. Thus, even though we work in a planar basis, we can use factorization to define physical connected parts with physical external particles. Figure 8.1 sketches a multiple-pole structure in a physical connected part that has been calculated

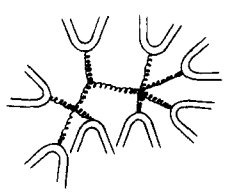

Fig. 8.1. Multiple-pole structure in a physical connected part calculated via factorization from the planar poles.

in the planar basis, i.e. with planar external particles. The residue structure in this example allows the extraction of 3-line, 4-line and 5-line physical connected parts.

Although we are aware of no argument that guarantees a one-to-one correspondence between planar poles and physical poles, there was implicit in the discussion of section 4 the assumption that a correspondence can be made between any planar particle and *some* physical particle. (When planar degeneracies occur, such as isospin degeneracy, it may be necessary to make the correspondence via linear superpositions of planar particles.) It is believed, in other words, that the physical asymptotic Hilbert space may be larger than the planar Hilbert space but not smaller. The simplest possibility – that the two spaces contain the same number of particles – remains open, both from a theoretical and an experimental point of view. No mesons have yet been discovered that cannot be put into correspondence with some planar meson.

Even should a one-to-one correspondence exist, we must learn how to deal with pole renormalization. The present section deals with one aspect of this question – related to the cylinder components. We are concerned with poles in a two-boundary cylinder, occurring in the channel invariant corresponding to the total (squared) energy flowing into one boundary and out the other, that is, "along the cylinder axis". For example in $M_0^{AB,CDE}$ we are concerned with poles in $s_{AB}=s_{CDE}$. According to the reasoning of section 7 these poles are also relevant to handles.

In formula (5.8) we exhibited the two-particle AB discontinuity of $M_0^{CD,AB}$. Veneziano observed that this complicated formula could be simplified by defining a quantity

$$\overline{M}_0^{CD,AB} \equiv M_0^{ABCD} + M_0^{BACD} + M_0^{ABDC} + M_0^{BADC} + M_0^{CD,AB}. \tag{8.1}$$

Remembering the planar discontinuity formulas, typified by (5.5), we find, following Veneziano [23],

$$\mathrm{disc}_{AB}\overline{M}_0^{CD,AB} = \overline{M}_0^{CD,EF} \otimes \overline{M}_0^{EF,AB}. \tag{8.2}$$

A straightforward generalization can be made for channels with any number of particles [13]. One defines $\overline{M}_0^{ABC\ldots,A'B'C'\cdots}$ as $M_0^{ABC\ldots,A'B'C'\cdots}$ *plus* the superposition of ordered amplitudes for all cyclic permutations *within* the two separate subsets. The general discontinuity formula for $\overline{M}_0$ then will have the structure of (8.2), a result that may be described as unitarity in a "cylinder Hilbert space", where the states are cyclically-symmetric superpositions of ordered channels, each channel satisfying the closed-boundary pattern of fig. 3.3. For example the 3-particle (A, B, C) state in the cylinder Hilbert space is

$$\frac{1}{\sqrt{3}}\left\{\left|\begin{matrix}A\\B\\C\end{matrix}\right\rangle + \left|\begin{matrix}B\\C\\A\end{matrix}\right\rangle + \left|\begin{matrix}C\\A\\B\end{matrix}\right\rangle\right\} \tag{8.3}$$

where the particle families are of the type $A(i,j)\,B(j,k)\,C(k,i)$. As noted earlier, cylinder channels are SU_N singlets in the presence of SU_N symmetry. The connected parts of the unitary "cylinder S matrix" are precisely the amplitudes $\overline{M}_0^{ABC\ldots,A'B'C'\cdots}$. Cylinder unitarity guarantees that the poles of these amplitudes should be factorizable. Comparing formula (8.1) to the full superposition of zero-handle components in the physical connected part $M^{A,B,C,D}$, as given by formula (5.2), and remembering the general rule about where poles may occur, we see that $\overline{M}_0^{CD,AB}$ subsumes all

the zero-handle components that are allowed to contain poles in s_{AB}.* By studying this quantity we therefore expect to learn about pole renormalization at the zero-handle level.

Discontinuity formulas of the type (8.2), which apply also to ordered and to physical connected parts, may be projected onto individual partial waves in angular momentum and schematically written in the matrix product form

$$M^+ - M^- = 2iM^-\rho M^+, \tag{8.4}$$

where M^+ and M^- are the same analytic matrix function M evaluated on opposite sides of the cut and ρ is a (diagonal matrix) phase-space factor. Equation (8.4) requires not only that the poles of M be factorizable but that poles on one sheet of the Riemann surface be matched by zeros in the determinant of $1 - 2iM\rho$ at corresponding points on the other sheet. Now if we express the generalization of eq. (8.1) as

$$\overline{M}_0 = P + C, \tag{8.5}$$

where P is the planar superposition specified above and C is the cylinder, then we see that it would only accidentally be true that zeros of $\det(1 - 2i\overline{M}_0\rho)$ would exactly coincide with zeros of $\det(1 - 2iR\rho)$, R being the matrix of ordered connected-part partial waves of which P is a particular linear superposition. In other words one does not expect poles of $\overline{M}_0$ at the positions of the ordered poles.

On the other hand we discussed in section 6 a systematic peripheral mechanism that is presumed to suppress the magnitude of the cylinder except at small values of the energy flowing along its axis. If the magnitude of C is small and that of P is not, the poles of $\overline{M}_0$ occur *close* to the zeros of $\det(1 - 2iP\rho)$, which one can show will be close to the poles of R. As the cylinder becomes weak, that is to say, the poles of $\overline{M}_0$ either approach the planar poles or their residues become small.

The reader may be perplexed at what is meant by the cylinder being "small" in the neighborhood of a pole of $\overline{M}_0$ which after all *also* must be a pole of C if it does not exactly coincide with one of the planar poles contained in P. The resolution of the puzzle is achieved by realizing that if $\overline{M}_0$ does not contain the planar poles, then C not only possesses the poles of $\overline{M}_0$ but must contain additional poles at the location of the planar poles of P – the additional poles exactly cancelling those of P. Speaking of a "weak" cylinder means, if P-pole residues are large, that there is close coincidence in both position and residue between a pole of $\overline{M}_0$ and a pole of P, so that in C the two corresponding poles almost compensate each other. Turning the argument around, if we accept the peripheral mechanism of section 7 as ensuring a weak cylinder component at high (positive) energy where planar poles are not negligible, then we require a near cancellation at high energy between pairs of cylinder poles.

Employing the Regge notion of simultaneous analyticity in energy and angular momentum one expects to be able to identify at any energy a correspondence between a Regge pole of $\overline{M}_0$** and that planar Regge pole which it will approach at high energy. Such an adiabatic connection

* To simplify the discussion we here assume that each of the four particles A, B, C, D carries nonzero internal quantum numbers so that none can appear alone on a single boundary. If one or more external particles carry zero quantum numbers, then in the order of the expansion considered in this section we must be prepared to identify cylinder renormalization of these external particles. It is unnecessarily confusing to consider simultaneously internal and external renormalizations. Factorization guarantees that if we understand one we also understand the other.

** It is speculated, although unproved, that the only Regge singularities of $\overline{M}_0$ (and C) in the axis-channel angular momentum are simple factorizable poles [24].

allows one to speak of pole "renormalization", even though the renormalization in position and residue may become large at low energy – the pole of $\overline{M}_0$ having very different properties from any planar pole.* Note that these large shifts are expected only for poles that communicate with channels in the cylinder Hilbert space, which we have seen to be a relatively small subset – SU_N singlets in the presence of SU_N symmetry.

The general considerations of this section will be given flesh and bone in the models discussed in sections 10 and 11, dealing with certain special leading poles. Because discontinuities of topological-expansion components with $h > 0$ never are bilinear in components with this same number of handles h, we do not again encounter for any individual component a discontinuity structure like formula (8.4) – demanding pole renormalization. So long as one works with a finite number of terms in the topological expansion, therefore, it is believed that the only renormalization is that discussed in the present section – of poles communicating with the two-boundary cylinder. It is believed at the same time, as explained in section 12, that the sum over an *infinite* number of handles will produce renormalization of *all* planar poles as well as a further renormalization of cylinder poles.** Both experimental evidence and the models reviewed in section 12 support the view that such general renormalization is quantitatively less important than the cylinder shift, which applies only to a modest subset of planar poles.

9. Multiperipheral bootstrap model of the ordered S matrix

The ordered unitary S matrix lies at the heart of the topological expansion; unless the concept S_0 makes sense the entire DTU approach is meaningless. The ordered S matrix not only provides the logical DTU underpinnings but specifies the planar approximation and all corrections thereto. Two intimately-related issues must be faced: (1) Does an analytic unitary S_0 exist? (2) How can S_0 be calculated?

The problem of existence is elusive because ordered unitarity, while simpler than physical unitarity, still implies an infinite set of nonlinear relations between ordered connected parts. No irreconcilable contradiction in these relations has been found but we remain far from a proof that a solution exists. So far all attacks on the ordered consistency (bootstrap) problem have focused on the presumed simplicity of Regge structure in ordered connected parts. Assuming that ordered Regge singularities are all factorizable poles, avenues of approach beckon that seem less promising for the full physical S matrix – where Regge cuts and fixed singularities abound. This section describes the most promising type of model so far developed for the ordered S-matrix bootstrap. The model is crude and represents only the beginning of what may be a long and arduous effort.

In section 6 it was asserted that ordered connected parts are large only in certain "strips". The model now to be described depends on this peripheral aspect of strong interactions, together with the assumption that contributions from a few leading Regge poles constitute a reasonable ap-

* For $t \to -\infty$, where t is the invariant mass squared flowing along the cylinder axis, one does not require the positions of $\overline{M}_0$ poles to approach the positions of planar poles even though the cylinder becomes weak, because here the residues of *both* sets of poles independently tend strongly to zero. Pole cancellation at negative t is not required in order to achieve peripheral strip structure for the cylinder.

** Reggeon calculus deals with the relatively small renormalization of the "bare pomeron" – the leading Regge trajectory of the cylinder.

proximation. We shall be led to self-consistency conditions on the parameters of leading ordered poles within strip regions.

Consider an n-particle intermediate-channel contribution to the discontinuity of the 4-line ordered connected part shown in fig. 9.1. (To avoid ambiguity we here mean *stable* particle when we say "particle".) One of the peripheral strips of large amplitude for the ordered amplitude associated with the reaction $\begin{pmatrix} C \\ A \end{pmatrix} \to \begin{pmatrix} 1 \\ 2 \\ \vdots \\ n \end{pmatrix}$ will correspond to the tree diagram of fig. 9.2. For small values of s_{AB} the other reaction occurring on the right-hand side of fig. 9.1 will be large in a corresponding strip. Other strips also exist, but the so-called "multiperipheral" strip of fig. 9.2 is expected to give the largest contribution in the limit $s_{AC} \to \infty$. Setting as our goal the determination of the leading ordered Regge poles in the $\begin{pmatrix} A \\ B \end{pmatrix} \to \begin{pmatrix} C \\ D \end{pmatrix}$ channel at small values of s_{AB}, it is then plausible to keep only the contribution from the multiperipheral strip.

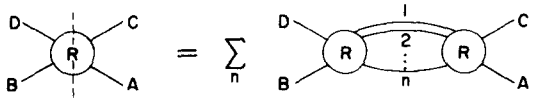

Fig. 9.1. An n-particle intermediate-channel contribution to the discontinuity of a 4-line ordered connected part.

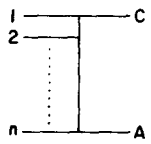

Fig. 9.2. Tree diagram corresponding to the multiperipheral strip of large amplitude for (C, A) → (1, 2, ... n).

A well-known property of the phase-space region corresponding to the multiperipheral strip is that rapidity ordering tends to coincide with particle ordering 1 ... n. Let us then divide the total phase space into two segments, assigning some fraction of the total rapidity interval between C and A to one segment and the remainder to the other segment. The fraction is unimportant; for definiteness we may divide the total interval into two halves. The important point is that among the n ordered intermediate particles the subset 1 to i tends to fall into one segment while the subset $i + 1$ to n tends to fall into the other. Now suppose that the average rapidity gap between particle i and particle $i + 1$ is large enough to allow factorized Regge representations of the form shown in fig. 9.3. Then performing the sum over all possible values of n is equivalent to performing *independently* the sums over all possible number of ordered particles within the two separate rapidity segments. By invoking ordered unitarity for 2-reggeon, 2 particle ordered amplitudes, we are led to the result shown in fig. 9.4, where it is to be understood that each of the two dis-

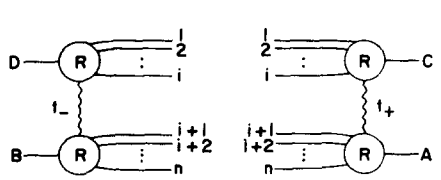

Fig. 9.3. A factorized Regge representation for the right-hand side of fig. 9.1.

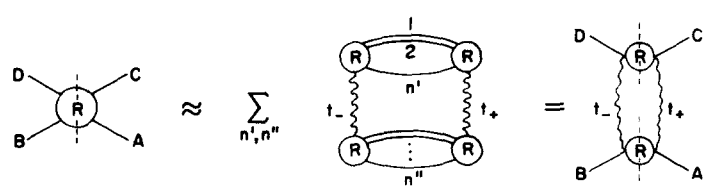

Fig. 9.4. The discontinuity of the 4-line ordered connected part expressed, via ordered unitarity, in terms of reggeon loop.

continuities appearing at the extreme right in fig. 9.4 is evaluated at a sub-s whose upper limit is proportional to $s_{AC}^{1/2}$, corresponding to its half of the total rapidity interval.

To the extent that the rapidity gap spanned by the reggeon may be small, it is necessary to sum over all possible reggeons – not simply the leading ones – but no investigators have so far seriously pursued this point of potentially profound consequences. The assumption has been made that the reggeon expansion converges rapidly, a good approximation being given by the highest-lying trajectories. Here we keep, for simplicity, only a single trajectory in the loop.

In the limit of large $s_{AC} \equiv s$ the left-hand side of fig. 9.4 will be dominated by the leading ordered reggeon with the quantum numbers of the AB channel, whose trajectory we designate by $\alpha(t)$, where $t \equiv s_{AB}$. If this reggeon has no physical particles for $J < 1$ ($J \equiv J_{AB}$), the point $J = 0$ being already a nonsense point as is the case for the leading physical reggeons, ρ, ω, f, A_2, then the discontinuity in question has the asymptotic structure

$$\frac{\gamma_{AB}(t)\gamma_{DC}(t)}{\Gamma(\alpha(t))} s^{\alpha(t)}, \tag{9.1}$$

the gamma function providing the sequence of zeros needed to prevent poles in the amplitude at nonsense points. The right-hand side of fig. 9.4 is more complicated, involving the product of discontinuities of reggeon-reggeon, particle-particle amplitudes. Consider the discontinuity involving the particles A and B, which we designate $A_{AB}(s', t, t_\pm)$ where s' is the square of the "cluster mass". In fig. 9.4 an integration is implied over the invariant s'. Because A_{AB} is the discontinuity of an ordered amplitude with Regge behavior in s' and supposedly with no Regge cuts, one expects this quantity to satisfy the sum rule [25]

$$\int_0^{s'_{max}} ds' A_{AB}(s', t, t_\pm) \underset{s'_{max}\to\infty}{\sim} \frac{\pi\gamma_{AB}(t)g(t, t_\pm)}{\Gamma(\alpha(t))} \frac{(s'_{max})^{\alpha(t)-\alpha(t_+)-\alpha(t_-)}}{\alpha(t) - \alpha(t_+) - \alpha(t_-) + 1}, \tag{9.2}$$

where $g(t, t_\pm)$ is the triple Regge coupling. There will be a similar sum rule for A_{DC}. We see then that in the equation of fig. 9.4 the dependence on the external particles factors out, leaving a condition involving only the leading ordered reggeon – a condition with the structure indicated in fig. 9.5.

Remembering that $s'_{max} \propto \sqrt{s}$, and using standard rules for the reggeon loop phase space together with the ordered single-reggeon propagator $(-s)^{\alpha(t_\pm)}\Gamma(1 - \alpha(t_\pm))$ one finds the schematic equation of fig. 9.5 taking the following explicit form, first written down by Rosenzweig and Veneziano [26]:

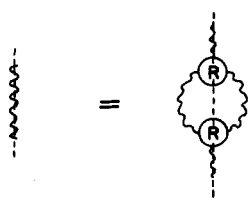

Fig. 9.5. The planar reggeon bootstrap equation.

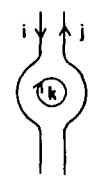

Fig. 9.6. Quark-line diagram for the right-hand side of fig. 9.5 with the closed quark loop responsible for the factor of N in eq. (9.3).

$$1 = \pi N \int \mathrm{d}\varphi \frac{S_0(t, t_\pm) g^2(t, t_\pm)}{(\alpha(t) - \alpha(t_+) - \alpha(t_-) + 1)} \tag{9.3}$$

where

$$S_0(t, t_\pm) \equiv \frac{\Gamma(1 - \alpha(t_+))\Gamma(1 - \alpha(t_-)) \cos \pi(\alpha(t_+) - \alpha(t_-))}{[\alpha(t) - \alpha(t_+) - \alpha(t_-) + 1]\Gamma(\alpha(t))} \tag{9.4}$$

is the ordered 2-reggeon loop "propagator". The factor N is the number of different equivalent ordered reggeon loops contributing to the right-hand side of fig. 9.5; with SU_N symmetry the quark-line diagram of fig. 9.6 shows that N flavors mean N loops. The loop phase space $\mathrm{d}\varphi$ in eq. (9.3) is

$$\mathrm{d}\varphi = \frac{1}{16\pi^4} \mathrm{d}t_+ \, \mathrm{d}t_- (-\lambda(t, t_+, t_-))^{-1/2} \theta(-\lambda) \tag{9.5}$$

with λ the usual triangle function.

The bootstrap equation (9.3) is a nonlinear condition on the trajectory and residue of the leading ordered reggeon. The trajectory is presumed to be a smooth function, but an infinite sequence of zeros and poles is anticipated in the triple-Regge coupling $g(t, t_\pm)$, as defined here. First it can be shown that there must be zeros at the points $\alpha(t) = \alpha(t_+) + \alpha(t_-) - n$, $n = 1, 2, \ldots$, if Regge branch points are not to occur in ordered amplitudes [25, 27]. At the same time it can also be shown that such zeros are redundant with propagator discontinuity zeros at $\alpha(t) = 0, -1, -2, \ldots$ when the helicities $\alpha(t_\pm)$ become physical integers and the triple reggeon coupling becomes a particle–particle–reggeon coupling. We thus expect $g(t, t_\pm)$ to have the form*

$$\frac{\Gamma(\alpha(t))}{\Gamma(\alpha(t) - \alpha(t_+) - \alpha(t_-) + 1)} \times \text{smooth function.} \tag{9.6}$$

With this assumption it is possible to find approximate solutions of the ordered bootstrap equation (9.3) that correspond reasonably with the experimentally observed properties of leading physical Regge trajectories. Before discussing quantitative matters, let us make a general observation.

Equation (9.3) or its physical equivalent has been derived by a variety of different approaches, many of which require great care in order to avoid miscounting intermediate states [1, 28–30]. Some of these alternative approaches have called attention to the remarkable nature of the requirement that Regge cuts be absent from ordered amplitudes. For such to be the case there must exist further sum rules going beyond that of eq. (9.2) [31]. At the time of this writing uncertainty continues about the full implications of the widely-employed assumption that the only Regge singularities of ordered amplitudes are factorizable poles [25, 27, 31, 32]. The reader should also remember that to achieve viable bootstrap equations *another* assumption is needed: dominance of the loop by a small number of leading ordered reggeons. There has been no proof of convergence of an expansion based on the location of ordered reggeons within the loop.

A less simple but more accurate approach to the ordered bootstrap has been made by Chan, Paton and Tsou (CPT) [1]. The physical idea is similar to the foregoing but in counting intermediate states use is made of the "cluster" concept which has proved useful in phenomenological

* Such a form is exhibited by the explicit triple-Regge coupling of the dual resonance model.

studies of experimental data. The CPT equations must be studied by computer, but it is correspondingly possible to be more realistic about kinematical facts of life. Each ingredient in the CPT equations has been thoroughly tested for physical meaning.

Numerical studies of equations of the general type (9.3) have been encouraging. It has been possible to satisfy eq. (9.3) over a range $1.0\ \mathrm{GeV}^2 \lesssim t \lesssim 1.0\ \mathrm{GeV}^2$ with a linear trajectory and a coupling of the form (9.6) [1, 33–35]. The leading intercept turns out to be $\alpha(0) \approx 0.5$ and the magnitude of the coupling is within a factor 2 of that indicated experimentally. The Rutherford Group [1] results, allowing more flexibility in the $t_\pm$ dependence, are even closer to experiment. Balazs, by using a modified and extended form of the bootstrap condition discussed here, has derived, with no free parameters, a reasonable infinitely-rising trajectory [35].

Of deep significance is the fact that ordered unitarity seems capable of determining both the positions and residues of poles. It appears, in other words, that the entire ordered S matrix may be determinable from self consistency. A puzzling question in this regard is how the breaking of SU_N symmetry will be fixed. A preliminary study by Konishi and Kwiecinski [36] has been based on combining a bootstrap equation of the "propagator" type of fig. 9.4 with one of the "vertex" type of fig. 9.7. It was found that for small symmetry breaking the pattern of trajectory intercepts must follow the "additive quark" rule:

$$\alpha_{ij} = \bar{\alpha} + \varepsilon_i + \varepsilon_j. \tag{9.7}$$

For the ordered triple-Regge coupling g_k^{ij}, corresponding to the quark-line diagram of fig. 9.8, where the discontinuity cuts the Regge pole, the other two legs corresponding to helicity poles, the pattern of small symmetry breaking is found to be

$$g_k^{ij} = \bar{g} + \eta_k. \tag{9.8}$$

The trajectory pattern (9.7), discovered earlier in a variety of less systematic theoretical studies [22, 37, 38], is in striking agreement with experiment. Experimental evidence about couplings is still too crude to check formula (9.8).

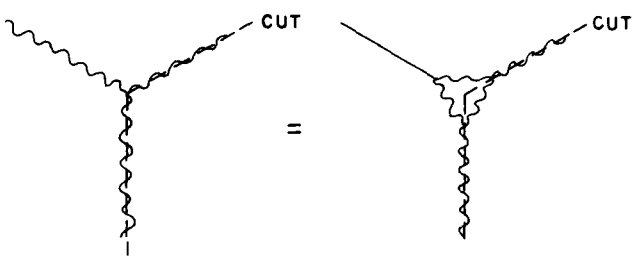

Fig. 9.7. Unitarity bootstrap equation for a three-reggeon vertex.

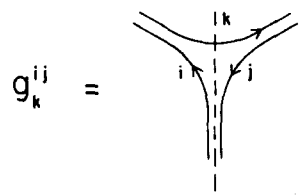

Fig. 9.8. Definition of the triple Regge coupling with respect to its indices in terms of a quark-line diagram.

A challenge *to* and opportunity *for* the DTU approach is the calculation of the symmetry breaking parameters ε_i and η_i. It would seem that ordered unitarity should determine these parameters of the ordered S matrix along with $\bar{\alpha}$ and $\bar{g}$. By the same token, ordered unitarity eventually should determine how many flavors occur. Before such questions can be answered, however, ordered bootstrap models must be vastly improved over the model-T versions currently available, which all have been modest adaptations of pre-DTU approaches. We are not yet close to exhausting the full content of ordered unitarity.

10. Multiperipheral model for leading cylinder poles

Section 8 dealt with general aspects of "axis-communicating" poles in the 2-boundary cylinder, using as a basis the discontinuity, cutting between the two boundaries, in the invariant that contains the poles. The present section describes a model of these same poles based on "boundary-slicing" discontinuities – in invariants formed by combining a portion of one boundary with a portion of the other. Historically it was models of this latter kind, directed at pomeron properties, that were in large part responsible for arousing interest in the topological expansion [39–41]. A remarkable variety of physical insights have emerged from boundary-slicing cylinder models.

According to standard Froissart–Gribov theory [5] the Regge singularities in J_{AB} – the angular momentum in a reaction AB → CD – are "built" from the discontinuities in s_{AC} and s_{AD}. One thus may hope to construct a model of the AB poles in $M_0^{AB,CD}$ in terms of the AC and AD discontinuities.* Since both discontinuities are nonvanishing, there is no exchange degeneracy; cylinder reggeons carry a signature label. We may nevertheless treat separately right-hand and left-hand cuts in the cosine of the angle conjugate to J_{AB}. Let us then proceed to consider the AC discontinuity of $M_0^{AB,CD}$.

The form of the two-particle contribution to a boundary-slicing discontinuity has been given in formula (5.6) but with a different assignment of particles to boundaries. With the present assignment we have for the EF contribution

$$\mathrm{disc}_{AC} M_0^{AB,CD} = M_0^{BEDF} \otimes M_0^{FCEA} + M_0^{BFDE} \otimes M_0^{ECFA}, \tag{10.1}$$

the first term on the right-hand side being depicted in fig. 10.1a, while fig. 10.1b indicates the generalization to an arbitrary multiparticle intermediate state. Note how the intermediate particles fall into two distinct ordered subsets.

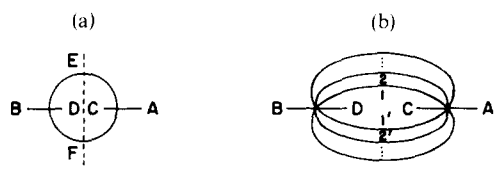

Fig. 10.1. (a) A two-particle contribution to a boundary-slicing discontinuity of the cylinder. (b) The generalization of (a) to a multiparticle intermediate state.

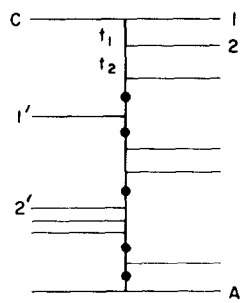

Fig. 10.2. The multiperipheral strip which is assumed to dominate the ordered amplitude appearing on the right-hand side of fig. 10.1b. The significance of the dots is explained in the text.

The leading J_{AB} singularities are related through the Froissart–Gribov projection to the asymptotic behavior of the AC discontinuity as $s_{AC} \to \infty$. Since each of the factors in an individual contribution to the cylinder AC discontinuity is an ordered connected part, whose asymptotic behavior is controlled by ordered reggeons, one hopes to relate the leading cylinder Regge singulari-

* Recall (section 6) that there are no poles of $M_0^{AB,CD}$ in the invariants s_{AC} and s_{AD}. Regge branch points in these channels play an important role in the considerations of section 11.

ties to the leading Regge poles of the ordered S matrix. It is necessary however to sum over an infinite number of individual contributions to the AC discontinuity.

Multiperipheral model

One assumes dominance by the multiperipheral strip of fig. 10.2, characterized by small magnitudes of the invariants $t_1, t_2, \ldots$. We have here a model analogous to the ordered bootstrap models discussed in section 9. The difference is that the ordering of the subset $1, 2, 3, \ldots$ is independent of the subset $1', 2', 3', \ldots$. In other words, we have as many different strips as tree graphs that interleave the two sequences in different ways. But if we assume for a particular tree graph (i.e. a particular strip) that the rapidity interval between a particle in one subset and a "neighboring particle" (in the sense of the tree graph) in the other subset is large enough to permit reggeon factorization at that link, then we can sum over all tree graphs (all strips) and obtain a simple result. Such an assumption is at least as justified as was the reggeon factorization that allowed construction in section 9 of the multiperipheral ordered bootstrap model. In both cases question must be raised about single-reggeon dominance of a modest rapidity interval.

In fig. 10.2 we have marked with dots those links in the Toller graph that join a particle in one subset with a particle in the opposite subset. Each way of distributing dots along the chain corresponds to a different strip. A possible way to perform the (triple) summation over the particles in each subset as well as the distribution of dots is to fix first the number of dots and sum over all possible numbers of particles between dots. Since by construction all particles between dots belong to the same ordered subset we are thereby performing the summation that yields the discontinuity of an ordered connected part. See fig. 10.3. The cylinder AC discontinuity then assumes the form shown in fig. 10.4, where an integration remains to be made over each reggeon loop between

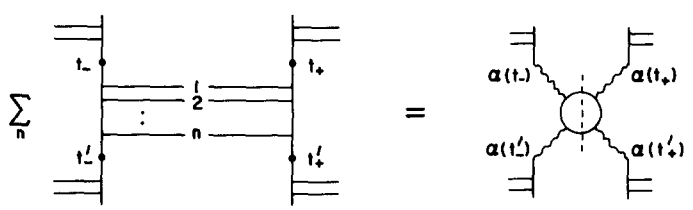

Fig. 10.3. Summation over subset of intermediate states which leads to a discontinuity of an ordered, four-reggeon connected part.

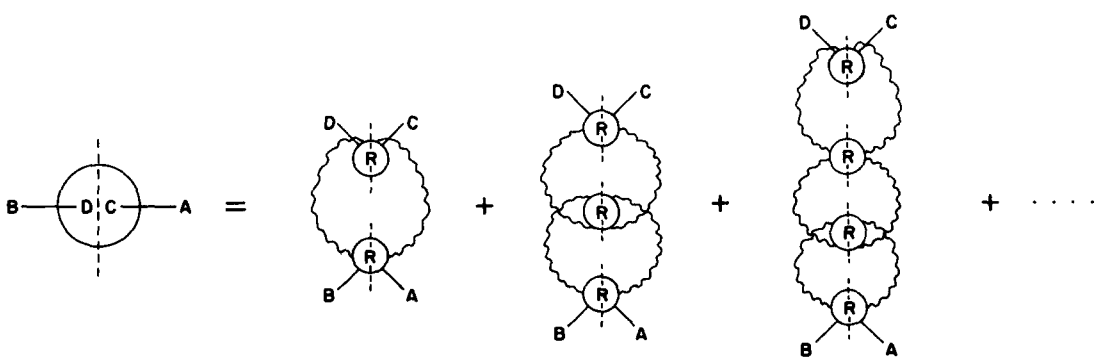

Fig. 10.4. The AC discontinuity of fig. 10.1 after the summation, as discussed in the text, over intermediate states is performed.

ordered clusters, the loop phase space being similar to that in fig. 9.4. Each cluster mass also is to be integrated over, but a significant difference between the equation represented in fig. 9.4 and the equation in fig. 10.4 is that for the former we had to restrict the rapidity interval covered by each ordered cluster so as to avoid double counting. There is no such restriction on the clusters in fig. 10.4; each is allowed to span the full kinematically-allowed range of cluster masses.

Charge conjugation and signature

What is the significance of the nonplanar-product ordering indicated for the reggeon products in fig. 10.4? In effect the order of lines in every alternate ordered discontinuity is reversed with respect to planar-product ordering. If it be recalled that the reggeons arose from links in Toller graphs between *nonadjacent* particles in ordered amplitudes one realizes that the reggeon propagators in fig. 10.4 should all be real; i.e., there are no associated discontinuities. Here is another significant difference between fig. 10.4 and fig. 9.4, where reggeon propagators carry a phase $e^{i\pi\alpha}$. A further significance of the ordering in fig. 10.4 relates to charge conjugation, as discussed in section 2. The rule presented [11, 12] was that reversal of order in an ordered connected part changes the phase by the product of charge-conjugation symmetry factors. Ordered reggeons do not have well-defined charge conjugation symmetry but they have well-defined values of the product of signature and charge conjugation symmetry. Let us call this parameter $\xi_i = \pm 1$. Combining the foregoing considerations into a single rule we may say that reversal of order in a reggeon ordered connected part changes the phase by the product of factors $\xi_i \exp(i\pi\alpha_i)$ for each reggeon. For physical particles this factor is just charge conjugation symmetry.

Using the foregoing rule we see that the first term on the right-hand side of the equation in fig. 10.4 differs from the corresponding planar product not only by the reggeon propagator phases $\exp\{i\pi[\alpha(t_+) - \alpha(t_-)]\}$ but by the charge conjugation symmetry of the AB → CD (cylinder axis) channel.* This term is positive for positive charge conjugation and negative for negative charge conjugation. The same will be true for all terms with an odd number of reggeon loops; those with an even number have the same value for both odd and even charge conjugation.

When the AD discontinuity is considered, the relative signs are such that positive signature carries positive charge-conjugation symmetry and negative signature carries negative charge-conjugation symmetry. Keeping track of charge conjugation will thus simultaneously identify signature.

Cylinder Regge poles

Examination of the series in fig. 10.4 reveals that for forward elastic scattering ($\bar{B} = A$, $\bar{D} = C$), where all terms are real and positive, the left-hand side must asymptotically grow with s_{AC} at least as fast as the discontinuity of an ordered connected part. The leading cylinder Regge singularity, in other words, cannot lie below α.

To understand as well as possible the leading cylinder singularities, let us now exploit the analysis in section 8 showing that pole structure is simplified if certain planar terms are added to the cylinder so as to form $\bar{M}_0^{AB,CD}$. Taking the s_{AC} discontinuity of $\bar{M}_0^{AB,CD}$, we are led to augment the right-hand side of the equation in fig. 10.4 by the ordered terms shown in fig. 10.5. It may now be recognized that if external particles are replaced by the reggeons appearing internally we have

* We here assume that the two reggeons forming a loop are the same so that $\xi_i\xi_i = 1$. Such need not always be the case. The leading $\xi_i = -1$ trajectory is the A_1.

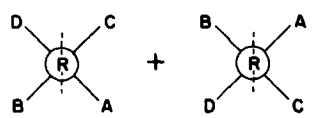

Fig. 10.5. An ordered term to be added to the discontinuity of fig. 10.4.

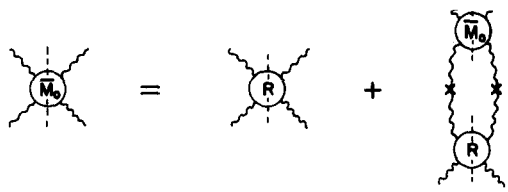

Fig. 10.6. The linear integral equation for the discontinuity of $\overline{M}_0$.

achieved a linear integral equation for the discontinuity of $\overline{M}_0$, where both the inhomogeneous term and the kernel are controlled by the four-reggeon ordered discontinuity. The structure of the equation is schematically indicated in fig. 10.6, where the crosses on the reggeon lines indicate the two phase requirements associated with order inversion: (1) The reggeon propagators are real. (2) The loop integral reverses sign when charge conjugation symmetry is reversed.

Diagonalizing the equation of fig. 10.6 with respect to axis-channel angular momentum will put it into Fredholm form [10] and allow the cylinder to be constructed from a knowledge of the ordered S matrix, even though the poles of the cylinder are shifted. The equation also can be solved by direct numerical iteration [1, 2]. Let us consider the pole-shifting phenomenon in terms of formal Fredholm theory. Suppose that projection has been made onto a definite (continuous) J, so as to yield a matrix function $\overline{M}_0(J,t)$ ($J = J_{AB}$, $t = s_{AB}$) in the space of a pair of ordered-reggeons.* The equation of fig. 10.6 then takes the operator form

$$\overline{M}_0(J,t) = R(J,t) + R(J,t)S_{cyl}(t)\overline{M}_0(J,t) \tag{10.2}$$

in the ordered reggeon Hilbert space. The operator $R(J,t)$ is analytic in J except for poles at $J = \alpha_i(t)$, the trajectories of the ordered reggeons; the singularity structure in t is standard. The twisted-loop "propagator" $S_{cyl}(t)$ is a diagonal operator in the 2-reggeon space whose form will be discussed below. Equation (10.2) may be formally solved to give

$$\overline{M}_0(J,t) = [1 - R(J,t)S_{cyl}(t)]^{-1}R(J,t) = [R(J,t)^{-1} - S_{cyl}(t)]^{-1}, \tag{10.3}$$

a result showing explicitly that $\overline{M}_0(J,t)$ is finite at the poles of $R(J,t)$, as expected from the more general argument in section 8. The poles of $\overline{M}_0(J,t)$ occur at points where

$$\det[R(J,t)^{-1} - S_{cyl}(t)] = 0, \tag{10.4}$$

points which systematically approach the positions of ordered poles when the "propagator" $S_{cyl}(t)$ tends to zero. In such a sense there will be a one-to-one correspondence between poles of $\overline{M}_0$ and ordered poles of appropriate quantum numbers. According to the multiperipheral model the cylinder shifts poles but does not create new ones [12, 42, 44].

Cylinder quenching

In sections 6 and 8 it was argued that the cylinder shift of ordered poles should approach zero as $t \to +\infty$. Within the model considered here, such an effect requires that $S_{cyl}(t) \to 0$ as $t \to +\infty$. Since the model is based on a low-t strip approximation it cannot be taken seriously for large t but one expects to see a tendency in the direction indicated by general arguments.

* The reggeons in this space correspond to helicity poles.

The cylinder loop propagator $S_{cyl}(t)$, a diagonal operator in the space of helicity poles, $\alpha(t_+)$, $\alpha(t_-)$, differs in two ways from the corresponding untwisted reggeon loop propagator in the multiperipheral ordered bootstrap (eq. 9.3): (1) S_{cyl} reverses sign when charge conjugation (or signature) is reversed, (2) S_{cyl} carries no factors $e^{i\alpha(t_\pm)}$. These differences translate in effect into the replacement of $S_0(t, t_\pm)$ as given in formula (9.4) by

$$S_{cyl}(t, t_+, t_-) = \pm \frac{S_0(t, t_+, t_-)}{\cos \pi(\alpha(t_+) - \alpha(t_-))}. \tag{10.5}$$

It is the inverse cosine factor, arising from reggeon phase change under order inversion that quenches $S_{cyl}(t)$ for large positive t.

To see this quenching it is convenient to change variables from $t_\pm$ to k and w according to

$$t_\pm = \tfrac{1}{4}t - k^2 - w^2 \pm w\sqrt{-t}, \tag{10.6}$$

the loop phase space in the new variables becoming

$$\int d\varphi = \frac{1}{8\pi^4} \int_0^\infty dk \int_{-\infty}^{\infty} dw. \tag{10.7}$$

For a linear leading ordered trajectory

$$\alpha(t) = \alpha(0) + \alpha' t \tag{10.8}$$

we then have

$$\frac{1}{\cos \pi[\alpha(t_+) - \alpha(t_-)]} = \frac{1}{\cosh 2\pi\alpha' w\sqrt{t}}, \tag{10.9}$$

which for positive t produces a quenching of the 2-reggeon "propagator". At negative t there is no quenching; a point to which we return below.

The reader may be puzzled by the fact that the function $S_0(t, t_\pm)$ was defined in eq. (9.4) to contain a cosine factor. How can it be claimed that quenching results merely by eliminating the cosine? The explanation can be given in either of two alternative forms:

(1) Formula (9.4) for $S_0(t, t_\pm)$ contains a product of gamma functions with the cosine factor, there being an important sense in which the product is simpler than the gamma functions alone. This sense relates to the requirement that ordered particle-pole residues all have the same sign; such a property is manifested by the *product*

$$e^{i\pi\alpha(t_+)}\Gamma(1 - \alpha(t_+))$$

but not by the gamma function alone – whose poles at $\alpha(t_+) = 1, 2, \ldots$ have residues that alternate in sign. Coherence of ordered poles is an essential facet of ordered unitarity; the coherent ordered propagator, if written in terms of a gamma function, *must* carry an additional alternating factor $(-1)^\alpha = e^{i\pi\alpha}$. By removing such a factor, residue sign alternation is generated [46, 47]. Such incoherence reflects a decrease in order when passing from the planar S matrix to the cylinder and makes the cylinder small for large positive t. One notes the similarity of such a mechanism to that producing "peripherality" (discussed in section 6): destructive interference between different angular momentum values.

(2) Since the ordered bootstrap equation (9.3), with a left-hand side independent of t, is supposed to hold over a *range* of t values the integrand on the right-hand side must *on the average* be independent of t; t dependence from the cosine factor in $S_0(J, t_\pm)$ must be compensated by t dependence from gamma functions. One then recognizes that a positive-t quenching tendency will result from removal of the cosine factor. The averaging notion will be exploited below to obtain a transparent formula for the cylinder shift of the leading planar pole.

Restriction to a finite number of ordered reggeons

The kernel of the cylinder integral equation (10.2) is determined by the ordered amplitude $(R(J, t)$, whose poles are factorizable. In consequence, if we approximate $R(J, t)$ by a finite number of Regge poles we achieve a kernel in the form of a finite number of factorizable terms. The integral equation then becomes equivalent to a set of linear algebraic equations coupling together the different ordered poles. In a vector space based on these poles let us define the diagonal pole matrix

$$P(J,t) = \begin{pmatrix} \dfrac{1}{[J-\alpha_1(t)]} & 0 & 0 & \cdots \\ 0 & \dfrac{1}{[J-\alpha_2(t)]} & 0 & \cdots \\ 0 & 0 & \dfrac{1}{[J-\alpha_3(t)]} & \cdots \end{pmatrix} \tag{10.10}$$

as well as the off-diagonal cylinder loop matrix

$$k_{nm}(t) = \pi \int \mathrm{d}\varphi \, S^{nm}_{\mathrm{cyl}}(t, t_\pm) g_n(t, t_\pm) g_m(t, t_\pm) \tag{10.11}$$

corresponding to the twisted quark-line diagram of fig. 10.7. The loop reggeons are understood to be the highest-lying ordered reggeons in the families appropriate to the involved vertices. The g_n are the corresponding ordered triple-Regge couplings. The cylinder equation then assumes the (finite) matrix form

$$\overline{M}_0(J,t) = P(J,t) + P(J,t)k(t)\overline{M}_0(J,t), \tag{10.12}$$

with the eigenvalue condition determining the cylinder poles:

$$\det\,[P^{-1}(J,t) - k(t)] = 0. \tag{10.13}$$

Fig. 10.7. Twisted quark-line diagram for the cylinder loop matrix.

Simple pole-shift formula with SU_N symmetry: emergence of the pomeron

Suppose only the leading SU_N multiplet of N^2 ordered poles is kept in approximating $R(J, t)$. With SU_N symmetry one may make superpositions corresponding to irreducible representations, and the cylinder will be found to couple only to the SU_N singlet. The corresponding cylinder pole, according to (10.13), is located at

$$J = \alpha(t) + \Delta\alpha(t) \tag{10.14}$$

where

$$\Delta\alpha(t) = Nk(t). \tag{10.15}$$

(With SU_N symmetry all N^2 elements of the matrix k are equal.) Comparing formulas (10.11) and (10.5) to (9.3) we see that*

$$\Delta\alpha^{\pm}(t) = \pm \left\langle \frac{\alpha(t) - \alpha(t_+) - \alpha(t_-) + 1}{\cos \pi[\alpha(t_+) - \alpha(t_-)]} \right\rangle, \tag{10.16}$$

the average being taken over the loop integral with the weighting function of (9.3). The plus sign goes with even charge conjugation symmetry and the minus sign with odd. The numerator of (10.16) increases linearly with t but the denominator increases exponentially, so the shift tends strongly to zero as $t \to +\infty$.

Formula (10.16) was first obtained at $t = 0$ and positive charge conjugation by Lee [39]. At this especially simple point where $t_+ = t_-$ we have

$$\Delta\alpha^{+}(0) = \alpha(0) - 2\langle\alpha\rangle + 1,$$

so the leading cylinder pole is located at

$$\alpha^{+}(0) = \alpha(0) + \Delta\alpha^{+}(0) = 1 + 2[\alpha(0) - \langle\alpha\rangle]. \tag{10.17}$$

Thus, if the strip width on the negative-t side is small so that $\langle\alpha\rangle \approx \alpha(0)$, one expects the leading cylinder pole to have the $t = 0$ properties of the pomeron: intercept near 1, even charge conjugation, positive signature and zero isospin.

Interpretation of the leading multiperipheral cylinder-model pole as the pomeron has not been universally accepted, because of the implication that the pomeron is the upward-shifted leading planar trajectory carrying the same quantum numbers as the pomeron. Such a trajectory, as we saw in section 4, contains as its first particle pole a good approximation to the f meson ($J^{PC} = 2^{++}$). According to the multiperipheral cylinder model, the pomeron trajectory contains the f meson; there is no separate f trajectory. A variety of arguments (which we comment on below) have been made to suggest that the pomeron should be a "new" singularity – not already contained in the planar spectrum. These arguments are insufficiently compelling, however, to require abandonment of the model described in this section. Having alerted the reader to a point of controversy, we continue to discuss the multiperipheral model's consequences.

Formula (10.16) turns out to be less meaningful for negative charge conjugation symmetry than for positive because of the influence of neglected lower-lying poles in $R(J, t)$. The direction of the cylinder shift of the leading odd charge conjugation pole is *downward*, bringing it into close

* The extra factor of $\alpha(t) - \alpha(t_+) - \alpha(t_-) + 1$ comes from the difference in the phase space integration between the planar and cylinder loops.

proximity with lower-lying poles. The calculation must then be expanded in order to be meaningful. With the availability of computers it is of course possible to avoid inessential approximations. We have discussed formula (10.16) because of its historical role with respect to the pomeron and because it exhibits so explicitly the magnitude of the cylinder shift, including the large-t damping.

The cylinder and SU_3 *symmetry breaking*

It was remarked in section 3 that the OZI rule takes on different aspects depending on whether SU_N symmetry breaking is large or small compared to deviations from planarity. Now that we have a model of the cylinder we can explore this subtle question. Let us assume that SU_2 symmetry is exact but that the breaking of SU_3 symmetry in the ordered S matrix is similar to that observed for the physical S matrix. We assume, in particular, on the basis of the observed mass difference between physical ω and physical φ (or between f and f') that the shift between leading ordered trajectories of the (n, n) or (p, p) class and those of the (λ, λ) class is about 0.4 units of J. We then have the interesting situation that for $t \lesssim 0$ the cylinder shift is comparable to or larger than SU_3 symmetry breaking while for large positive t the cylinder shift is smaller. We now describe a simple model that allows study of the transition between these two regimes.

Suppose that in $R(J, t)$ we keep the leading poles in *each* of the 3 families (n, n), (p, p) and (λ, λ). To achieve maximum simplicity let us follow ref. [42] and assume that symmetry breaking of the ordered pole positions in P is more important than symmetry breaking of the cylinder coupling coefficients k. Such a simplifying assumption, although inessential, is consistent in spirit with the general pole-dominance approach; all nine cylinder elements are then approximated by a single number $k(t)$. SU_3 symmetry breaking is entirely characterized by the ordered-trajectory spacing $\Delta(t)$

$$\alpha_1(t) = \alpha_2(t) = \alpha_3(t) + \Delta(t), \tag{10.18}$$

the displaced trajectories and associated eigenvectors being determined by the ratio between $k(t)$ and $\Delta(t)$. This ratio, that is to say, determines the degree of OZI-rule violation. Models of this type have been extensively studied in the literature; we now describe the qualitative lessons that have been learned.

At large positive t where $k(t)$ is smaller than $\Delta(t)$, the cylinder shift of each ordered trajectory not only is small but the coupling shifts are also small. After projection on $I = 0$, the underlying ordered Hilbert space becomes reduced from three states to two, f $-$ f' for even charge conjugation and $\omega - \varphi$ for odd charge conjugation. The coupling shift may consequently be characterized for each pole by a "mixing angle", giving the superpositions of the two ordered states that constitutes the associated eigenvector of Pk. Cylinder mixing angles are zero in the limit $k \to 0$ corresponding to f and ω being purely of the type $[(\mathrm{p}, \mathrm{p}) + (\mathrm{n}, \mathrm{n})]/\sqrt{2}$ while f' and φ are purely of the type (λ, λ). The mixing angles are proportional to $k(t)$ for small $k(t)$ and grow in magnitude as t diminishes. Trajectory shifts also grow with $k(t)$; f and f' trajectories are displaced upward while ω and φ trajectories are displaced downward. The sign of the mixing angles is such that f and φ move in the direction of becoming SU_3 singlets as the ratio k/Δ grows, while ω and f' tend to become SU_3 octets. All estimates agree that near $t = 0$ the magnitude of k/Δ is of the order unity so that the eigenvectors are roughly halfway between the ordered (sometimes called "ideal") limit and the "strong cylinder" limit corresponding to irreducible representations of SU_3. Most models predict that as t becomes more and more negative the ratio k/Δ will continue to increase, making SU_3 symmetry more and more accurate for cylinder-communicating poles.

The latter point can be confusing because, according to the peripheral strip hypothesis (section 6) the cylinder amplitude $M_0^{AB,CD}$ is small except for small values of $|t| = |s_{AB}|$. However, the cylinder amplitude is proportional to $k(t)$ only for small k; the cylinder coupling $k(t)$ may be large even though the cylinder amplitude is small. The quantity $k(t)$ controls the shift of a trajectory and its SU_3 content but does not control the magnitude of the Regge residue, which throughout maintains the same order of magnitude as the ordered residues.

All the foregoing features find at least qualitative support from experiment, as discussed in refs. [48–51]. We have seen in formula (10.16), which is an approximation to $\pm 3k$, that the magnitude and sign of k at $t = 0$ is satisfactory. Assigning to k a roughly exponential variation with t,

$$k(t) \propto e^{-t/t_c}, \tag{10.19}$$

with the "cylinder-quenching interval" $t_c \approx (\alpha')^{-1}$, semi-quantitatively correlates such diverse experimental facts as the pomeron slope, the $f - A_2$ mass difference, the difference between πp and Kp high energy elastic differential cross sections as a function of t, and the deviation of φ from ideal mixing. (The latter point is treated further in section 11.) If the averaging indicated in formula (10.16) is carried out with the ordered triple-Regge couplings that satisfy the ordered bootstrap equation (9.3), one indeed finds for small $|t|$ a t-dependence close to (10.19) [19, 34, 45, 51]. The multiperipheral model of the cylinder thus appears in good shape from an experimental standpoint.

Pomeron-f identity

The pomeron-f identity is a source of uneasiness about the cylinder model described in this section. Many physicists are troubled, partly because of the phenomenological successes [52] of the Harari-Freund picture employing exchange-degenerate ρ, f, A_2, ω *plus* a pomeron, and partly because of QCD expectations of "glueballs" – states made of gluons rather than quarks. (The highest glueball trajectory is expected to have the quantum numbers of the pomeron.) We are not deeply concerned about the latter viewpoint as such, partly because no reliable way yet exists to evaluate the QCD predictions for glueballs and partly because the poles of the ordered S matrix should not be viewed as literal $q\bar{q}$ composites. The quark-line diagrams of the DTU program are merely representations of ordered relationships. We are more concerned about reasoning by Veneziano [53], stimulated by QCD but *within* the DTU framework, which calls attention to the artificial nature of the reggeon links in the equation of fig. 10.4. Veneziano points out, for example, that particle 1′ in fig. 10.2 can resonate with particle 2′, even though these particles appear in two separate clusters in the equation of fig. 10.4. Veneziano urges that in neglecting such correlations, the distinctive character of the pomeron may have been lost. We have two remarks in response to Veneziano's concern: (1) The same criticism of artificial separation may be made of the ordered bootstrap model. Particles in the first cluster in fig. 9.3 actually can resonate with particles in the second cluster. Factorization on a reggeon link is a questionable feature of *any* multiperipheral model; it does not seem to us especially dangerous for the cylinder model. In fact, because the definition of the strip region of fig. 10.2 demands rapidity ordering, the requirement that at least one particle of the opposing subset stand in rapidity *between* particles 1′ and 2′ means that the rapidity gap between the latter will on the average be *larger* than the rapidity gap separating the two clusters of fig. 9.3. Reggeon factorization may thus be a *better* approximation for the cylinder model than for the ordered model. The neglected correlations should in principle be accounted for by including nonleading reggeon exchanges. While one expects these lower trajectories to change the quantitative results, whether they will change the results qualitatively, as Veneziano

suggests, is an open question [54, 55]. (2) The physical picture of the pomeron as the shadow of multiperipheral-dominated production processes, emerging from the above model, coincides with the bulk of particle-production phenomenology. More detailed models, making contact with this phenomenology, find the f intercept to be shifted from near 0.5 to near 1.0.

So far as the phenomenological successes of the Harari–Freund picture are concerned, we believe that the multiperipheral cylinder model has already gone further in explaining experimental facts.* In addition, the general unitarity arguments of section 8 show that the f *cannot* survive – maintaining its ordered position and residue – when the cylinder is added. Even if the pomeron is a new singularity, with no counterpart in the planar spectrum, cylinder unitarity still requires the f to undergo a substantial shift.

Unnatural parity

Although not yet as well understood, the cylinder shift of leading unnatural parity trajectories deserves mention. Employing the multiperipheral model in the same spirit as for natural parity, one expects shifts of the four $I = 0$ trajectories η, η', H and H′ away from the $I = 1$ π and B trajectories [58–60]. The magnitude of $k(t)$ needed here to explain the experimentally-observed shift of η and π is similar to that for natural parity, but the sign of the required cylinder loop coupling is reversed. The latter fact has been explained by Millan through the nonidentity of the two ordered reggeons in the loop [61, 62]. Unnatural-parity within the cylinder is clouded by uncertainty concerning unnatural parity at the planar level. Because the two ordered reggeons within the leading loop here have different trajectories (having opposite naturality), reggeon phase factors play a role qualitatively different from that for purely natural parity. Finding a consistent ordered triple-Regge coupling $g(t)$ is tricky when there is a displacement between the two helicity poles [34]. It is plausible that solution of the problem will involve a dynamical zero physically related to the Adler zero, since the most successful dual resonance models of $\pi\pi$ amplitudes have contained such zeros when the spacing between π and ρ trajectories is approximately 0.5 [6]. At the time of this writing, a consistent unnatural-parity multiperipheral ordered bootstrap model remains a tantalizing goal. When such a model is achieved, the corresponding cylinder model will unambiguously follow.

11. Cylinder violation of OZI selection rules

Section 10 has discussed the breaking of isospin and exchange degeneracy – cylinder violations of planar regularities. Also discussed have been the coupling shifts of ordered reggeons away from the "ideal" ordered limit – another departure from the maximal regularity of the planar S matrix. We did not, however, explicitly discuss the violation of OZI selection rules, for the reason that most of the experimental evidence regarding the latter requires going outside the low-t strip – into a region not describable by the multiperipheral model. The latter model does describe the transverse structure of the low-t strip cylinder damping resulting from pole-residue sign alternation in reggeon propagators. Nevertheless, large positive t requires an understanding of two other, quite different,

* Careful comparison with experiment requires attention to threshold effects, as emphasized especially by Dash and collaborators [56, 57].

strips. The present section will describe a large-t model based on Regge branch points in the cylinder.

The reader should remember that we are continuing here to deal with the same component of the topological expansion as formed the subject of sections 8 and 10; the discontinuity formula underlying our analysis of cylinder unitarity will also form the basis for the Regge-cut model. In moving from small t to large t, physical emphasis shifts from Regge-pole properties to the violation of OZI selection rules, but both categories of physical effects are controlled by the cylinder. With the aim of firming this bridge in the reader's mind, we begin the present section by explicitly relating OZI-rule violating decays of φ and f' to a rough but conceptually useful notion introduced in section 10 – that of mixing angles.

Mixing angles

Approximating the cylinder through only two ordered poles such as φ and ω (odd charge conjugation) or f' and f (even charge conjugation) allows pole-residue shifts to be represented by a mixing angle. The coupling in the multiperipheral model is to the set of channels that dominate the ordered bootstrap, but the same mixing angle applies to all channels. In conventional quantum-mechanical notation one expresses such a notion by writing

$$|\varphi_{\text{cyl}}(t)\rangle = \cos\theta^-(t)\,|\varphi_{\text{ord}}(t)\rangle + \sin\theta^-(t)\,|\omega_{\text{ord}}(t)\rangle, \tag{11.1}$$

$$|\omega_{\text{cyl}}(t)\rangle = -\sin\theta^-(t)\,|\varphi_{\text{ord}}(t)\rangle + \cos\theta^-(t)\,|\omega_{\text{ord}}(t)\rangle, \tag{11.2}$$

with a corresponding pair of formulas for f_{cyl} and f'_{cyl} in terms of an angle θ^+. These formulas arose in describing ratios of couplings to the dominant 2-reggeon loops in the multiperipheral equations. For example

$$M(\text{f}'_{\text{cyl}} \leftrightarrow \rho^+_{\text{ord}} + \rho^-_{\text{ord}}) \approx \sin\theta^+(m^2_{\text{f}'})M(\text{f}_{\text{ord}} \leftrightarrow \rho^+_{\text{ord}} + \rho^-_{\text{ord}}) \tag{11.3}$$

but in an approximation based on only two ordered poles the same angle $\theta^+(m^2_{\text{f}'})$ also describes the relative couplings of f' and f to $\pi^+\pi^-$. The measured ratio between the OZI forbidden decay $\text{f}' \to \pi\pi$ and the allowed decay $\text{f} \to \pi\pi$ then translates into a value of θ^+.

The notion of a single angle to describe *all* coupling ratios for a pair of trajectories can at best be a rough approximation, since many more than two ordered poles communicate through the cylinder, but as a way of compactly characterizing certain types of OZI-rule violation, the mixing angle concept is widely employed.* We shall often in this section, for example, refer to the experimentally-measured value of $\theta^-(m^2_\varphi)$, based on the ratio of the forbidden decay $\varphi \to \rho + \pi$ to the allowed decay $\omega \to \rho + \pi$, tacitly treating $\theta^-(m^2_\varphi)$ as an intrinsic property of the physical φ – independent of the channel to which φ may be coupled.

We have discussed how, in the cylinder multiperipheral model, the mixing angles $\theta^\pm(t)$ are proportional to twisted loop integrals when the latter are small. For example, in the simplified model of section 10 that was characterized by the single ratio $k(t)/\Delta(t)$, one finds [42]

$$\theta^\pm(t) \approx \pm\sqrt{2}\,k(t)/\Delta(t). \tag{11.4}$$

Although at large t the multiperipheral model eventually loses validity, one may continue quali-

* One important difference in our use of the mixing angle is that we explicitly consider the t-dependence (mass-dependence) of mixing angles.

tatively to think of OZI-rule violation in terms of mixing angles, and it may be hoped that at the physical φ and f' masses – on the "fringe" of the strip – formula (11.4) maintains qualitative significance.* In section 10 we pointed out that the small measured values of $\theta^-(m_\varphi^2)$ and $\theta^+(m_{f'}^2)$ are compatible through formula (11.4) with the large pomeron-f shift at $t = 0$ if $k(t)$ is an exponentially decreasing function. One of the special virtues of (11.4), which so far as we know is not shared by other models, is that it correctly predicts the signs of the mixing angles $\theta^+(m_f^2)$ and $\theta^-(m_\varphi^2)$ in addition to their magnitude.

If the mixing-angle concept is applied to the unnatural-parity $\eta - \eta'$ system, experimental measurements imply that $\theta^+(m_\eta^2)$ and $\theta^+(m_{\eta'}^2)$ are much larger [58, 59, 66] than the corresponding mixing angles for natural parity. The smallness of the η mass leads us here to expect large deviation from ideal coupling, but the substantial deviation observed for η', even though $m_{\eta'}^2 \approx m_\varphi^2 \approx 1\ \mathrm{GeV}^2$, implies a slower cylinder quenching rate for unnatural parity than for natural.** Put differently, the low-t strip appears to be broader when the cylinder carries unnatural parity. Nevertheless the $\eta - \eta'$ system can be successfully described in terms of mixing angles, with the t-variation (i.e. $\theta^+(m_\eta^2) > \theta^+(m_{\eta'}^2)$) now very important [58, 59].

Regge-cut model of the cylinder

To handle large values of t, outside the strong low-t cylinder strip, a model has been proposed by Veneziano [23] and by Chan, Kwiecinski and Roberts [67], that is based on the *other* two cylinder strips, which are weaker because of the absence of parallel poles but which nevertheless dominate $M_0^{AB,CD}$ as $s_{AB}(t) \to \infty$ at either fixed s_{AC} or fixed s_{AD}. Cylinder-communicating states of high mass but low angular momentum may then be considered.

The model rests on the discontinuity (5.8), cutting between cylinder boundaries, that formed the basis of section 8. For present purposes, assuming the cylinder to be weak for large s_{AB}, we neglect all terms in the discontinuity formula that contain the cylinder itself and keep only products of ordered amplitudes, i.e. four terms of the type shown in fig. 11.1. Two of these terms tend to populate the strip where s_{AC} is small and two populate the strip where s_{AD} is small. We focus attention on the former. Let us tentatively assume that the intermediate-particle cluster $(1, 2, \ldots n)$ tends to be separated in rapidity from the cluster $(1', 2', \ldots n')$, so that the link between the clusters may be represented by the leading reggeon with appropriate quantum numbers. Summing over particles within the two separate clusters then leads to the approximation schematically indicated in fig. 11.2. Remembering the strip structure of ordered amplitudes discussed in section 6 (see fig. 6.3), we see that for small $s_{AC} = s_{BD}$ the separate ordered discontinuities appearing on the right-hand side in fig. 11.2 are large only when their other channel invariants are also small. The cluster masses, in particular, tend to be small – confirming a posteriori the assumption of a large intercluster rapidity gap. As in previous models one must integrate over cluster masses, but ordered

* The multiperipheral cylinder model contains a mechanism, also deducible from general unitarity arguments [19, 63–65], that in effect gives an imaginary part to the mixing angle. In the loop integral there occur channel thresholds, associated with poles of the reggeon propagators, and careful evaluation produces an associated imaginary part of $k(t)$ for t above these thresholds. Physically one may say that φ (or f') decays into $K\bar{K}$ which then makes a transition via ω (or f) to $\pi\rho$ (or $\pi\pi$), each of the two processes in this succession being allowed at the planar level. The effect turns out to be relatively small because ordered resonance decay widths are small compared to the $\omega - \varphi$ (or f – f') mass differences. Additionally, when many channels are "open", interchannel cancellations result from the alternating signs of pole residues.

** As remarked at the end of section 10, no calculation of the unnatural-parity cylinder loop integral can be made until the corresponding ordered triple-Regge couplings have been determined from the ordered unnatural-parity bootstrap.

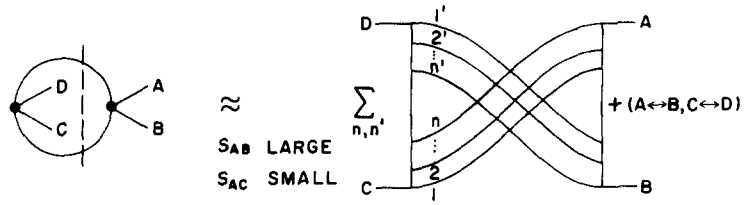

Fig. 11.1. Product of ordered amplitudes contributing to the AB discontinuity of the cylinder.

peripheral strip structure sharply confines the mass interval from which significant contributions arise.

As $s_{AB}(t) \to \infty$ the product in fig. 11.2 has the power behavior

$$s_{AB}^{\alpha_+(t_+)+\alpha_-(t_-)-1};$$

that is to say, the leading Regge singularity in the AC → BD channel is a branch point at $J_{AC} = \alpha_+(t_+) + \alpha_-(t_-) - 1$. The product is small for two reasons – corresponding respectively to the location of the branch point and to the associated discontinuity: (1) First of all, for s_{AC} small the power of s_{AB} corresponding to the Regge cut is less than that corresponding to an ordered

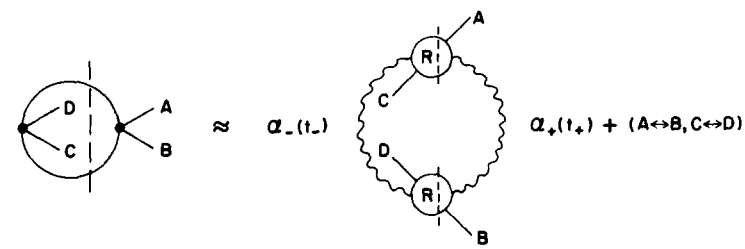

Fig. 11.2. A reggeon loop approximation to the cylinder discontinuity depicted in fig. 11.1.

pole. Consider the quark-line diagram associated with fig. 11.2, shown in fig. 11.3(a) in comparison to an ordered diagram, fig. 11.3(b). At $s_{AC} = 0$ the leading power for the ordered amplitude in the large s_{AB} limit is $\alpha_{kj}(0)$, where α_{kj} is the leading reggeon in the (j, k) family, whereas the leading power for the cylinder is $\alpha_{kj}(0) + \alpha_{il}(0) - 1$. The power difference is $1 - \alpha_{il}(0)$, ensuring that asymptotically a cylinder amplitude becomes negligible compared to the corresponding planar amplitude, if $\alpha_{il}(0) < 1$. (2) Even were $\alpha_{il}(0)$ close to 1, the cylinder would be weak because outside the low-s_{AB}

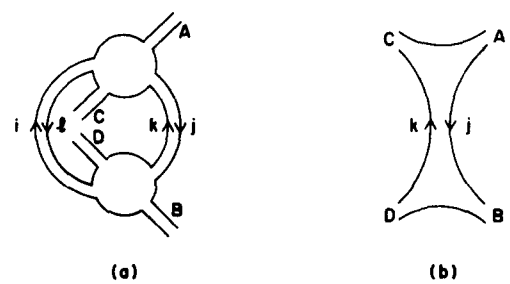

Fig. 11.3. (a) The quark-line diagram corresponding to fig. 11.2. (b) A quark-line diagram for an ordered connected part, to be compared to (a).

strip the cluster-mass integrals on the right-hand side of fig. 11.2 are numerically small, corresponding to the smallness of the Regge-cut discontinuity. Smallness of these cluster-mass integrals is related to smallness of the peripheral strip width, which in turn is related to destructive interference from different values of angular momentum. That is, by keeping small the *nonadjacent* channel invariants s_{AC} and s_{BD} in the ordered discontinuities of fig. 11.2, we are in effect evaluating these quantities near "backward" directions as the cluster mass attempts to grow. Factors of $(-1)^J$ are correspondingly present. The integral over an ordered discontinuity with a fixed *nonadjacent* channel invariant is often characterized by a dimensionless parameter ε [46, 47, 68, 69]. The strength of the Regge cut is proportional to ε^2, most estimates agreeing that $\varepsilon^2 \lesssim 0.1$. To summarize, in the Regge-cut model the order of magnitude of the cylinder-planar ratio at large t and low s_{AC} is

$$\varepsilon^2(\alpha' t)^{\alpha_{il}(0)-1}, \tag{11.5}$$

assuming the energy scale to be set by the slope of leading ordered trajectories.

Chan et al. [67, 70] have employed the Regge-cut model to explain a variety of qualitative experimental observations concerning charmonium decay. We may appreciate the nature of their considerations by examining the already-discussed parallel problem of the "strangeonium" decay $\varphi \to \rho + \pi$. Choose the particles A and B to be K^+ and K^-, with an order such that a (λ, λ) family enters one cylinder boundary. Let particles C and D be π^+ and ρ^-, with an order such that a (p, p) family exits from the other boundary. Project then on $J_{AB} = 1$ and make the semilocal duality assumption that the smooth discontinuity given by the Regge-cut representation corresponds to an average over resonances in the AB → CD channel. Knowing the resonance spacing, the Regge-cut model thus yields $J = 1$ pole residues, and one factor of the φ residue corresponds to the desired coupling $\varphi \to \rho\pi$.

According to formula (11.5), the ratio of the latter OZI-violating coupling to an allowed coupling is of order

$$\varepsilon^2(\alpha' m_\varphi^2)^{\alpha_{\lambda p}(0)-1}. \tag{11.6}$$

Since $\alpha' m_\varphi^2$ happens to be close to 1, we find the Regge-cut model of the cylinder predicting the mixing angle $\theta^-(m_\varphi^2)$ to be of the order ε^2. Such a statement sounds completely different from (11.4) – the multiperipheral model result. Is it accidental that both models agree with experiment ($\theta^-(m_\rho^2) \approx 0.1$ radians)?

Relation between multiperipheral and Regge-cut models

The φ mass happens to lie in the transition region – on the outer fringe of the low-t strip and at the beginning of the high-t interval where semi-local duality gives meaning to crossed-channel Regge representations. Although both multiperipheral and Regge-cut models are here being stretched to their limits of validity, there is precedent for supposing that an overlap region exists where high-t and low-t approximations are simultaneously meaningful. It is furthermore the case that in both models the smallness of the predicted mixing angle is attributable to $(-1)^J$ destructive interference.

The fact that the multiperipheral model yields an exponential decrease of cylinder strength while the Regge-cut model yields a power decrease is understandable through the strip structure of fig. 6.4. The former model is concerned with the strong low-s_{AB} strip while the latter concerns itself with the weak ($\sim\varepsilon^2$) strips at low s_{AC} and low s_{AD}. The exponential behavior refers to the

transverse structure of the strong strip while the power behavior refers to the longitudinal structure of the weak strips.

OZI-rule violation in 4-line connected parts

As an example of OZI-rule violation that cannot completely be expressed through a mixing angle, consider the two-boundary cylinder component $M_0^{A,BCD}$ for a reaction forbidden at the planar level, where particle A and only particle A has quantum numbers allowing communication with the cylinder axis. An illustration might be $A = \varphi$, $B = \pi^0$, $C = \pi^+$, $D = \pi^-$. There are poles in all three channel invariants s_{AB}, s_{AC} and s_{AD}, with three corresponding strip regions. When only one invariant is small and the other two large, a single strip is important and one may use a representation in terms of the ordered Regge poles parallel to this strip. Roughly speaking, the only difference in this region from a corresponding ordered amplitude (nonvanishing in the same strip) is a mixing-angle factor. In our $\pi^+\pi^- \to \varphi\pi^0$ illustration if we go to the strip where s_{AB} is large and s_{AC} is small, the leading Regge pole is ρ^+ and the ratio to the allowed amplitude $\pi^+\pi^- \to \omega\pi^0$ is just the ratio of the Regge couplings $\rho^+(s_{AC}) - \pi^+\varphi$ to $\rho^+(s_{AC}) - \pi^+\omega$, which we expect to be of order ε^2.* The situation, however, is more complicated in the region where all three invariants s_{AB}, s_{AC} and s_{AD} are small.

In this central region of the Mandelstam diagram the singularity structure of $M_0^{A,BCD}$ is qualitatively different from that of an ordered connected part such as M_0^{ABCD}, which has poles in only two of the three invariants. Crude models of this central region, based on the discontinuity formula (5.7), suggest that where all three strips converge the amplitude $M_0^{A,BCD}$ becomes comparable in magnitude to an ordered amplitude. Only when the energy is high enough to allow contributions from many different intermediate channels does $(-1)^J$ destructive interference reduce the cylinder magnitude [72–74].

12. Torus

Cylinder corrections to the planar S matrix are expected on the basis of the two convergence mechanisms discussed in sections 6 and 7 to be more important than corrections involving handles. According to experimental observations, as described in section 4, such seems indeed to be the case; the most visible departures from planar regularities involve cylinder-communicating channels. Small irregularities are nevertheless inevitable in *all* channels as a result of $h \neq 0$ components of the topological expansion. This section considers the component with one handle and one boundary – commonly described as a "torus" – that is expected to constitute the most significant $h \neq 0$ correction.

As explained in section 7 such a component will be smaller than the corresponding planar component by a "statistical" factor $1/N^2$, N being the average number of flavors allowed by phase space to be effective in intermediate states. We have interpreted the $1/N^2$ factor as manifesting the constraint that only SU_N singlet channels are allowed to flow through handles. Additionally, as explained in section 6, intermediate handle-traversing channels are constrained by peripheral

* As shown by Kwiecinski [71] the mixing angle $\theta^-(m_\varphi^2)$ is strictly-speaking relevant only to the physical points on the rho trajectory where $\alpha_\rho = 1, 2, \ldots$.

dynamics to be of low energy. The combination of these two suppressive mechanisms ensures relative smallness for the torus.

Speaking loosely, if one associates the pomeron with the cylinder and regards a handle as an "internal cylinder", one may say that adding a handle is like adding an internal pomeron link. A connection is then recognized between the summation over many handles and Gribov's reggeon calculus, which is a generalization of the idea of "absorptive" correction through pomeron insertions. The weakness of pomeron couplings, on which reggeon calculus depends, is seen as a manifestation of the convergence mechanisms within the topological expansion. The connection between DTU and reggeon calculus has been studied by Ciafaloni, Marchesini and Veneziano [16]. We shall not venture into this arena, restricting our attention to a simpler although physically-related question that requires only a single handle: the torus shift of planar trajectories.* A lesson will emerge: The shift cannot be calculated in terms of pomeron couplings. The handle structure is more subtle.

Crossed-channel torus discontinuity

Suppose we wish to correct the ordered AB-channel Regge poles of M_0^{ABCD} by adding M_1^{ABCD}. We assume the isospin of the AB channel *not* to be $I = 0$, so there is no communicating cylinder component. As usual we may think of AB poles as arising from AC and AD discontinuities. Now a correction to the AD discontinuity will not disturb the standard planar regularities, since this discontinuity is already nonzero in the ordered amplitude. Odd and even signatured trajectories, in particular, receive a common shift from a torus contribution to the AD discontinuity; there is no breaking of exchange degeneracy [75]. On the other hand, with the torus contribution to the AC discontinuity, exchange degeneracy *is* broken, so we concentrate attention on the AC discontinuity of M_1^{ABCD}.

The discontinuity formula turns out to involve two classes of terms: planar times planar and planar times cylinder. The former appears first in a 3-particle discontinuity, while the latter appears in a 2-particle discontinuity. Understanding as usual that intermediate "particles" are ordered clusters, we have

$$\begin{aligned}\mathrm{disc}_{AC} M_1^{ABCD} = {} & M_0^{BFEDG} \otimes M_0^{AGFCE} + M_0^{BEDFG} \otimes M_0^{AGCEF} + M_0^{BF,DE} \otimes M_0^{AFCE} \\ & + M_0^{BEDF} \otimes M_0^{AF,EC}. \end{aligned} \tag{12.1}$$

When s_{AC} is large and s_{AB} is small the planar times planar terms are large in the doubly-peripheral strip indicated in fig. 12.1. Representing intercluster rapidity gaps by reggeons and summing over clusters, we are led to the approximation of fig. 12.2 for the planar times planar portion of the torus AC discontinuity. Applying the reasoning that led us in fig. 11.2 to conclude that both cluster masses there were limited leads here to the conclusion of a limited central-cluster mass. Each of the two end clusters in fig. 12.2 is unrestricted in mass,** however, and one cannot argue for a large rapidity gap between clusters.

* Strictly-speaking, a single-handle component does not by itself shift a pole but generates a double pole at the same position. It may nevertheless be shown by standard renormalization considerations that the double pole is the first of an infinite correlated sequence of multiple poles, the pole order increasing with the number of handles and the series summing to a shifted pole: $\sum_{h=0}^{\infty} \Delta^h/(J-\alpha)^{h+1} = 1/(J-\alpha-\Delta)$. Understanding the single-handle (double pole) term thus yields the shift Δ.

** Two unrestricted clusters corresponds to the statement (preceding footnote) that the J_{AB} projection has a double pole as its leading Regge singularity.

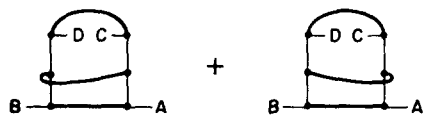

Fig. 12.1. Product of tree diagrams, indicating the strips where the amplitude is expected to be large. Darker lines represent clusters.

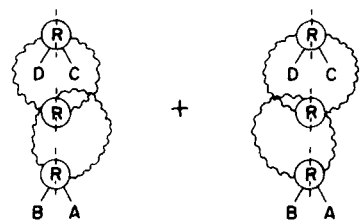

Fig. 12.2. Reggeon loop approximation for fig. 12.1.

Some investigators have at this point followed the spirit of the multiperipheral ordered and cylinder models where reggeon links were employed for small as well as large rapidity gaps [47, 68, 76]. Other investigators [77, 78] have invoked techniques from reggeon calculus in an effort to include the effect of the central cluster's merging into one of the end clusters. There is unresolved controversy about which approach gives the more reliable result. All investigators agree on the order of magnitude (see below), but the sign is in question. In any event one should not ignore those terms in formula (12.1) that involve the cylinder.

The cylinder times planar contribution is indicated in fig. 12.3 and corresponds to two ordered clusters, each of unrestricted mass. No reliable calculation has yet been made of this contribution, but estimates indicate that near $t = s_{AB} = 0$ the cylinder times planar terms are comparable to the planar times planar [79]. Indeed, our experience with formula (5.8) suggests that simplification of the calculation may result by considering simultaneously the two sets of terms. Certainly, if the cylinder contribution is adequately to be evaluated, one must not forget those cylinder poles that precisely cancel $I = 0$ planar poles.

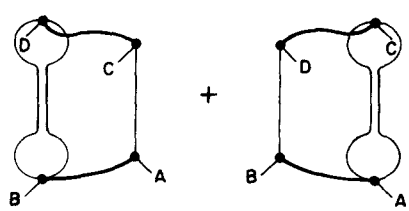

Fig. 12.3. The cylinder times planar contribution to the crossed channel torus discontinuity. Darker lines represent clusters.

The small magnitude of the planar times planar portion of the torus AC discontinuity follows partially from the smallness of the integral over the central (twisted) cluster in fig. 12.2. Characterizing the smallness of this integral by the parameter ε used to characterize the twisted cluster integral in fig. 11.2, the order of magnitude of the ratio of a torus discontinuity to a corresponding ordered discontinuity is estimated to be $\varepsilon/N_{\text{eff}}^2$. When translated into a trajectory shift, an angular momentum displacement of this same order is anticipated, which for $N_{\text{eff}} \approx 2.5$ and $|\varepsilon| \sim 0.3$ is indeed the experimentally-observed order of magnitude – as seen in fig. 4.1. A convincing quantitative calculation of the trajectory shift, however, has not yet been achieved through the crossed-channel discontinuity [79].

Direct-channel torus discontinuity

The shift of an AB ordered pole is in some respects easier to understand through the AB torus discontinuity than through the AC discontinuity [80]. The two-particle (two ordered cluster) discontinuity involves the four cylinder times planar terms shown in fig. 12.4.* The intermediate cluster E, because it attaches by itself to an isolated boundary of a cylinder, must have $I = 0$ and contain pairs of poles that tend to cancel each other, with the residual difference between the two shrinking as their mass increases. We have discussed how the largest difference occurs for the lowest-mass $I = 0$ particles. Thus we may approximate the E cluster, which may be thought of as "the handle", by a rapidly converging sequence of cylinder-shifted particles minus the corresponding planar particles. The dominant contribution should be $\eta - \eta_{\text{planar}}$ which, to the extent that η_{planar} is degenerate with π, we may approximate as $\eta - \pi$. For all other physical particles the cylinder shift is extremely small.

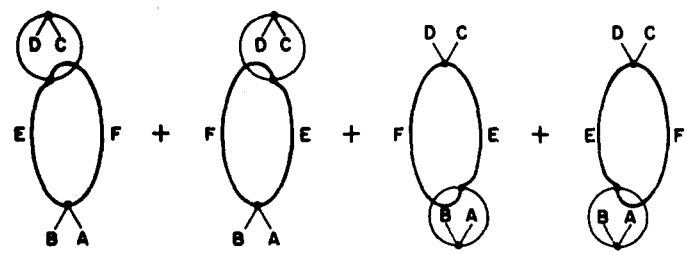

Fig. 12.4. Cylinder times planar contribution to the direct channel torus discontinuity. Darker lines represent clusters.

The link F must carry the internal quantum numbers of the AB channel (which we have agreed is not $I = 0$), and the residues of poles in both E and F links alternate in sign with J (or with charge conjugation). Both links, that is to say, can be shown to be "twisted" in the same sense as were the links in the reggeon loops of the multiperipheral cylinder model.

Suppose we are interested in $\rho - A_2$ trajectory splitting, so $I_{AB} = 1$. The leading poles in the F link then have isospin 1 and appear with the relative signs $\pi - B$, $A_2 - \rho$, etc. Correspondingly, the lowest-mass contributions to the AB torus discontinuity carry the relative coefficients

$$(\eta - \pi)(\pi - B + A_2 - \rho). \tag{12.2}$$

Such a superposition of intermediate states is precisely that dictated by G-parity conservation, which we emphasized in section 2 is not obeyed by intermediate states at the planar level. Consider, for example, the terms in formula (12.2) that correspond to pairs of pseudoscalar mesons:

$$\eta\pi - \pi\pi. \tag{12.3}$$

G parity allows $\eta\pi$ to communicate with A_2 but not with ρ, while the reverse is true for $\pi\pi$, so the *difference* of the discontinuities contributing to A_2 and ρ, with observance of G parity, will contain the combination (12.3). It can be shown that the complete structure of the torus two-particle AB discontinuity, including the sign alternation with charge conjugation, may be deduced from the G-parity requirement on states that do not communicate with the cylinder [80].

* We ignore the torus times planar terms and the planar times planar terms which enter at the 3-particle level. The latter should to a large extent be incorporated through our use of cylinder poles for the E cluster.

If one assumes that the trajectory displacement

$$\alpha_{A_2}(t) - \alpha_\rho(t) \tag{12.4}$$

vanishes smoothly as $|t| \to \infty$, satisfying an unsubtracted dispersion relation in t, a calculation of the displacement may be based on the measured partial widths for the decays $A_2 \to \pi\eta$, $\pi\rho$, $\rho \to \pi\pi$, $\pi\omega$, etc. into the two-particle channels represented in (12.2).* When such a calculation is performed, the lowest-threshold AB-communicating intermediate two-particle channels give a semi-quantitative account of the $A_2 - \rho$ displacement, explaining the sign, the magnitude and the derivative [80]. The dominant contribution arises from the $\pi\pi$ channel, which because it contributes to ρ and not to A_2, lifts the former above the latter.

The success of the direct-channel dispersive calculation gives empirical support to the conjecture that a trajectory-difference such as (12.4) should satisfy an unsubtracted dispersion relation – implying that at large negative t as well as at large positive t the trajectories smoothly approach each other. (Inhibition on high-mass flow through a handle may be the source of convergence.) The calculation of the torus through its direct-channel discontinuity is then much easier than through the crossed channel.** The mechanisms ensuring a small torus magnitude operate in either approach.

13. Baryons and baryonium

The success of DTU in describing mesons encourages search for a generalization. Dual models, the nonunitary forerunners of DTU, were early constructed for baryons with moderate success [6]. It was quickly realized by Rosner [81] that duality for baryons implies a new particle family corresponding in quark-diagram language to $qq\bar{q}\bar{q}$ – a combination of two quarks with two antiquarks. Such exotic particles would necessarily communicate strongly with baryon-antibaryon channels, and it was conjectured that there would be only weak coupling to the ordinary $q\bar{q}$ mesons. For many years the absence of experimental support for these exotics caused doubt about the relevance of dual models to baryons, but recently evidence has begun to accumulate [82] for a class of high-mass narrow resonances with zero baryon number produced in reactions where baryon–antibaryon combinations occur. Assuming these new states to be the long-sought Rosner exotics, they have tentatively been dubbed "baryonium" [83].

To date it has not been established that any baryonium state carries quantum numbers such as $I = 2$ that cannot be carried by a nonexotic $q\bar{q}$ meson. Until such characteristically-exotic quantum numbers are established, there will remain doubt about the theoretical status of the new particle family. Nevertheless, the impetus to extend DTU has been increased by the recent explosion of baryonium candidates. There is presently a big theoretical push to find an OZI-rule generalization capable of explaining the stability of baryonium states through a mechanism analogous to that stabilizing strangeonium and charmonium [84].

Further experimental impetus to extend DTU comes from the observation of approximately exchange-degenerate patterns for certain baryon trajectories [6]. It is plausible that such regulari-

* Unitarity relates the imaginary part of a trajectory to the width of the physical-particle states occurring on the trajectory [5].

** We are here assuming that it will eventually be possible to compute in the planar plus cylinder approximation the various relevant three-particle couplings (e.g. $\rho - \pi\pi$, $A_2 - \pi\eta$, etc.). Up to the present time, as emphasized at the end of section 9, there exist no ordered or cylinder models for unnatural-parity particles.

ties are a manifestation of an ordered S matrix, just as we have seen to be the case for nonexotic mesons. Last but far from least, there is the experimental fact that many baryon properties can be understood in terms of a qqq structure. It is tempting to seek an explanation through order, just as we did for the $q\bar{q}$ meson properties through a sequentially-ordered S matrix.

What should be expected from a generalization of the DTU approach described in sections 2, 3 and 5? The central desired feature is an ordered unitary S matrix whose factorizable poles provide basis for a sequence of approximations that systematically approach a unitary physical S matrix. We expect the ordered S matrix to display special regularities – degeneracies and selection rules, among these being the $q\bar{q}$ meson regularities already discussed; one of the additional regularities should be an ordered-pole subset with qqq properties. A candidate for an ordered S matrix with such attributes has recently been found [85, 86]. A somewhat related concept of order is discussed in ref. [87].

Generalization of the sequentially-ordered S matrix

The order introduced in section 2 assigns to each particle a predecessor and a successor; each particle is "connected" to two other particles. Suppose we allow any number of interparticle connections and try to define a unitary ordered S-matrix – acting in a Hilbert space of ordered channels. It turns out that most connection patterns are incompatible with unitarity. The most general unitarizable pattern so far found implies a spectrum of ordered particles that bears encouraging resemblance to the observed spectrum of hadrons.

Represent with a graph the connection pattern within an ordered amplitude, the labeled vertices of the graph corresponding to the poles (particles) of the ordered S matrix. The graph edges represent interparticle connections, a "tadpole" edge connecting a vertex to itself not being admitted. Sequentially-ordered amplitudes correspond to "ring" graphs such as shown in fig. 13.1(a). More general connections are illustrated by (b)...(e) in the same figure. We know that connections of type (a) are admitted by ordered unitarity. What about (b)...(e)? It turns out that (d) is allowed but (b), (c) or (e) are not. Why?

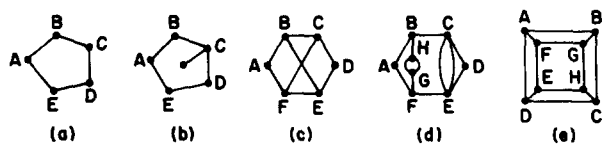

Fig. 13.1. Candidate amplitude graphs representing connection patterns between particles. Only graphs a and d represent connections admitted by ordered unitarity.

For an amplitude to correspond to a transition between two ordered channels, the specification of the channel pair must determine uniquely the amplitude. The most natural and only known way to accomplish this end is to associate ordered channels with those graphs achieved by cutting amplitude graphs into two connected portions. (Looking back at section 2 the reader may verify the associability of sequentially-ordered channels with connected graphs cut away from ring graphs.) There should furthermore be a unique prescription for recombining the two channel graphs to form the amplitude graph. Since each vertex corresponds to a particle, the pole-factorization aspect of unitarity demands that any vertex of an amplitude graph be isolatable by a cut that leaves connected the remainder of the graph. This requirement immediately eliminates graphs

with "pendant" vertices, illustrated by fig. 13.1(b). In this example the vertex C cannot be isolated by a legal cut. Other aspects of unitarity eliminate many other types of graph.

To make a long story short the only amplitude graphs so far found to be consistent with unitarity are those without pendant vertices that, when split in all possible ways into two connected portions, always yield channel graphs with unique "spanning trees". A spanning tree of an arbitrary graph is a tree graph reached by successively removing edges to eliminate cycles (closed loops), at each stage eliminating any vertex at which two and only two edges have a junction.* Figure 13.2 shows the spanning trees of some graphs that can be formed by cutting the graphs of fig. 13.1. Notice that only the graphs in the (a) and (d) groups have unique spanning trees. These graphs are of the type that corresponds to ordered channels.**

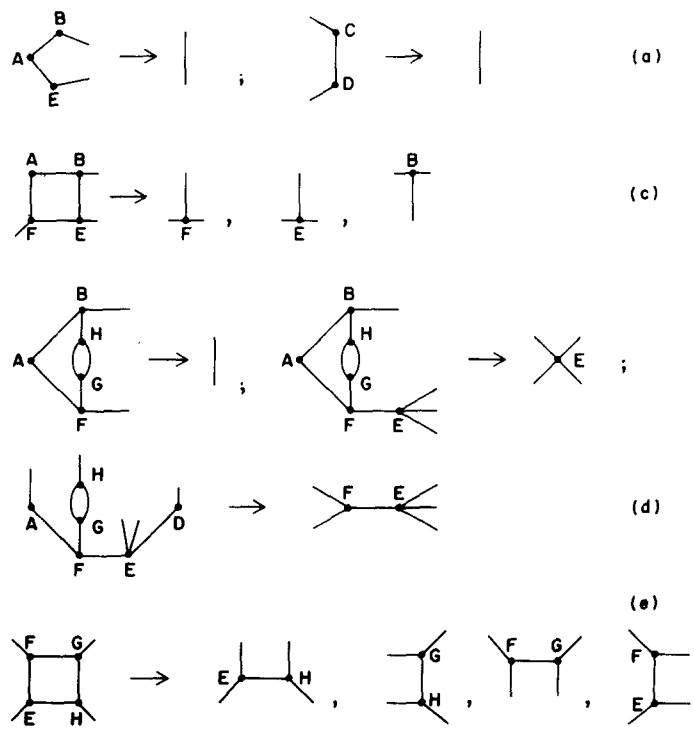

Fig. 13.2. Spanning trees for various cuts of the amplitude graphs of fig. 13.1. Only graphs a and d lead to unique spanning graphs.

Color

To achieve the essential objective that a pair of channel graphs be recombinable (into an amplitude graph) in only one possible way, it turns out that graph edges must be colored. With the appropriate coloring there then is a unique prescription for imbedding graphs on a spherical surface. Precisely *three* colors turn out to be required! Although the connection between DTU

* If tadpoles are created in the process, they are to be erased, together with the connecting edge.

** It can be shown that ordered amplitudes correspond to graphs that are reducible to rings by repetition of the following contractions: (1) Replace by a single edge any set of edges that connect the same pair of vertices. (2) Remove 2-vertices.

color and QCD color is not yet understood, we have here an outstanding instance of promised physical illumination from DTU. Many qualitative features of the DTU approach are potentially understandable from QCD, but the Lagrangian approach so far gives no hint of the number of colors needed to describe strong interactions. The number 3 arises in DTU because within graph theory the 3-vertex plays a special role.

It is natural to assume symmetry under interchange of different colors. In passing from the ordered S matrix to a planar S matrix (in the sense of section 2), it is expected that the color degree of freedom will disappear as the Hilbert space is contracted to eliminate order. This contraction has not been exhaustively investigated, but let us proceed to consider the spectrum of ordered particles assuming it to be coincident with the planar spectrum – the situation prevailing for sequential ordering.

The ordered-particle spectrum

Analysis of ordered unitarity reveals a splitting of the ordered Hilbert space into a collection of noncommunicating sectors, each sector being characterized by a colored spanning-tree skeleton (imbedded on a planar surface) with 3-vertices only. The simplest skeletons are shown in fig. 13.3, the three colors being indicated by numbers 1, 2, 3. The communicating channels within a given sector are those whose spanning trees share the skeleton in question; communicating poles (particles) are naturally labeled by their sector skeleton.

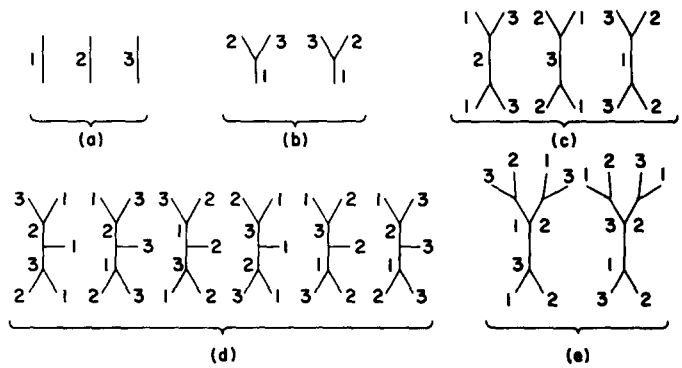

Fig. 13.3. Spanning tree skeletons for the most simple sectors of the ordered Hilbert space. The three colors are indicated by the numbers 1, 2, 3.

Replacing each particle vertex in an amplitude graph by the appropriate sector skeleton, one achieves a graph containing only 3-vertices. Two classes of vertex occur (when the graph is imbedded on a spherical surface): those with clockwise color order (1, 2, 3) and those with counterclockwise color order. Adjacent vertices can be shown to have opposite orientation, so in an amplitude graph there are equal numbers of each orientation. One may then assign a conserved quantum number $+1$ to the clockwise 3-vertex, with the counterclockwise 3-vertex carrying -1; it is natural to associate this conserved quantity with baryon number. We then see that ordered S-matrix sectors (a) and (c) in fig. 13.3 carry baryon number zero, sectors (b) and (d) carry baryon number ± 1, while sector (e) carries baryon number ± 2. Sectors evidently exist with indefinitely-high baryon number. It is natural to associate ordered particles of sector (b) with ordinary (nonexotic) baryons

and ordered particles of sector (a) with nonexotic mesons. Particles in sector (c) presumably correspond to baryonium, while those in (d) constitute a class of exotic baryons.

Contact with quark language can be made by attaching a direction to each edge according to the orientation of the 3-vertices connected by the edge. Choosing the conventional edge direction to be *away* from the clockwise oriented vertex *toward* the counterclockwise-oriented vertex, we may, if we choose, say that the edge *carries* baryon number 1/3 and think of the edge as a quark.* The various sectors shown in fig. 13.3 might then be characterized as in fig. 13.4. Note that the ordered S matrix does not tolerate "single-quark" or "two-quark" sectors. All states have integer baryon number. (Single-quark states were eliminated by the unitarity inhibition on pendant vertices.)

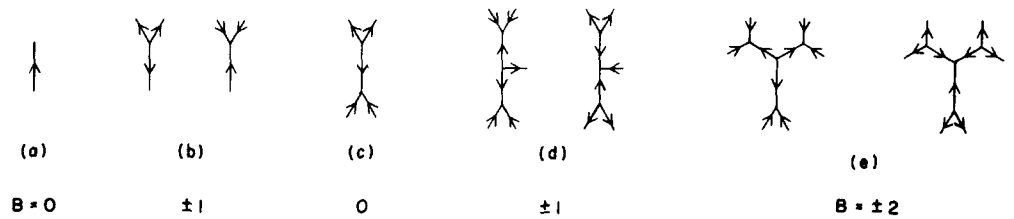

Fig. 13.4. Characterization of the sectors of fig. 13.3 in quark diagram language. The arrows represent the flow of baryon number 1/3.

Ordered baryonium states (type (c)) do not communicate with type (a) ordered meson states. There is similar absence of communication between type (d) ordered exotic baryons and type (b) ordered baryons. The desired extension of the OZI rule has thus been achieved. The ordered S matrix has furthermore generated qqq structure for (type (b)) baryons in an exchange-degenerate pattern, while maintaining $q\bar{q}$ structure for ordinary mesons.**

Conclusion

The future of the DTU approach at this point looks bright. Many questions remain unanswered but substantial portions of the quark picture have emerged as manifestations of an ordered relationship between S-matrix poles. The topological expansion based on sequential ordering has explained the existence and properties of the pomeron at the same time as providing a quantitative description of OZI-rule violations. In the most general order so far found to be compatible with unitarity, a hint has appeared of the necessity and sufficiency of 3 colors. There has not yet been developed for the general S matrix the equivalent of section 5's meson-sector topological expansion, so there can presently be no claim to understanding the mechanisms that may suppress corrections to the general planar S matrix. In particular we do not at this juncture know how, even in principle, to calculate the width of baryonium states. The accelerating rate of recent progress nevertheless makes promising the outlook for a bootstrap theory of hadrons keyed to ordered relationships.

This progress rate foretells a short useful lifetime for our review. Ideas that have been described here will soon be generalized, simplified and their logical inter-relationship reorganized. Mathe-

* Weissmann, by generalizing the considerations of section 3, has shown that flavors also behave as if carried along the directed edges [7].

** Within the $q\bar{q}$ sector all the regularities of the sequentially-ordered S matrix are preserved, even though this sector includes communicating ordered channels with baryon–antibaryon pairs.

matical tools of which we are presently unaware will shortly be brought to bear on the augmentation of S-matrix theory by the concept of order. We accept this fate for our effort, having no choice in the matter. If this review succeeds in engaging the interest of a few physicists previously unaware or unimpressed by the DTU approach, we count our effort worthwhile.

Acknowledgments

Many colleagues have assisted in the preparation of this review. Especially worthy of mention are Yoav Eylon, Philip Lucht, Jean-Pierre Sursock, George Weissmann, Fritjof Capra and Henry Stapp.

References

[1] Chan H.M., J.E. Paton and Tsou S.T., Nucl. Phys. B86 (1976) 479.
[2] Chan H.M., J.E. Paton, Tsou S.T. and Ng S.W., Nucl. Phys. B92 (1975) 13.
[3] G. Veneziano, Nucl. Phys. B74 (1974) 365; Phys. Lett. 52B (1974) 220.
[4] A.D. Martin and T.D. Spearman, Elementary particle theory (North-Holland, Amsterdam, 1970).
[5] P.D.B. Collins and E.J. Squires, Regge poles in particle physics (Springer-Verlag, Berlin, 1968).
[6] M. Fukugita and K. Igi, Phys. Reports 31C, No. 4 (1977).
[7] G. Weissmann, Ph.D. thesis, University of California at Berkeley (1978).
[8] J.R. Taylor, J. Math. Phys. 7 (1966) 181.
[9] J.P. Sursock and P. Lucht, unpublished, Berkeley (1977).
[10] P. Lucht, Ph.D. thesis, University of California at Berkeley (1977).
[11] Y. Eylon, Phys. Rev. D13 (1976) 3317 and Lawrence Berkeley Laboratory report LBL-6736.
[12] C. Schmid and C. Sorensen, Nucl. Phys. B96 (1975) 209.
[13] G.F. Chew and C. Rosenzweig, Annals of Phys. (N.Y.) 105 (1977) 212.
[14] S. Okubo, Phys. Lett. 5 (1963) 165;
G. Zweig, unpublished;
J. Iizuka, Suppl. Prog. Theor. Phys. 37–38 (1966) 21.
[15] S. Okubo, Phys. Rev. D16 (1977) 2336.
[16] M. Ciafaloni, G. Marchesini and G. Veneziano, Nucl. Phys. B98 (1975) 472, 493.
[17] J. Edmonds, Notices Amer. Math. Soc. 7 (1960) 646;
See also J.W.T. Youngs, J. Math. Mech. 12 (1963) 303–315 and
A.T. White, Graphs, groups and surfaces (North-Holland, 1973) p. 61.
[18] J.P. Sursock, Ph.D. thesis, University of California, Berkeley (1978).
[19] G.F. Chew and C. Rosenzweig, Nucl. Phys. B104 (1976) 290.
[20] J.E. Paton and Chan H.M., Nucl. Phys. B10 (1969) 516.
[21] A.T. White, Graphs, groups and surfaces (North-Holland, 1973).
[22] N. Papadopoulos, C. Schmid, C. Sorensen and D. Webber, Nucl. Phys. B101 (1975) 189.
[23] G. Veneziano, Nucl. Phys. B108 (1976) 285.
[24] J.R. Freeman, University of Nebraska preprint (1977).
[25] J.R. Freeman, G. Veneziano and Y. Zarmi, Nucl. Phys. B120 (1977) 477.
[26] C. Rosenzweig and G. Veneziano, Phys. Lett. 52B (1974) 335.
[27] M. Bishari and G. Veneziano, Phys. Lett. 58B (1975) 445.
[28] J. Finkelstein and J. Koplik, Phys. Rev. D14 (1976) 1437.
[29] J.R. Freeman and Y. Zarmi, Nucl. Phys. B112 (1976) 303.
[30] J. Kwiecinski and N. Sakai, Nucl. Phys. B106 (1976) 44.
[31] J.R. Freeman and C.E. Jones, Phys. Rev. D16 (1977) 1932, 1936.
[32] J. Kwiecinski and N. Sakai, Nucl. Phys. B127 (1977) 87.
[33] M. Schaap and G. Veneziano, Lett. Nuovo Cimento 12 (1975) 204.
[34] J. Millan, Ph.D. thesis, University of California at Berkeley (1977), LBL 7235.

[35] L.A.P. Balazs, Phys. Rev. D15 (1977) 319 and Phys. Lett. 71B (1977) 216.
[36] K. Konishi and J. Kwiecinski, Nucl. Phys. B125 (1977) 264.
[37] J. Dias de Deus and J. Uschersohn, Physica Scripta 14, no. 2 (1976) 19.
[38] K. Konishi, Nucl. Phys. B116 (1976) 356.
[39] H. Lee, Phys. Rev. Lett. 30 (1973) 719.
[40] G. Veneziano, Phys. Lett. 43B (1973) 413.
[41] Chan M.H. and J.E. Paton, Phys. Lett. 46B (1973) 228.
[42] G.F. Chew and C. Rosenzweig, Phys. Lett. 58B (1975) 93; Phys. Rev. D12 (1975) 3907.
[43] N. Sakai, Nucl. Phys. B99 (1975) 167.
[44] L.A.P. Balazs, Phys. Lett. 61B (1976) 187.
[45] M. Bishari, Phys. Lett. 59B (1975) 461.
[46] C. Schmid, C. Sorensen and D.M. Webber, Nucl. Phys. B111 (1976) 317.
[47] Y. Eylon, Nucl. Phys. B118 (1977) 95, 119.
[48] P. Stevens, G.F. Chew and C. Rosenzweig, Nucl. Phys. B110 (1976) 335.
[49] C.B. Chiu, M. Hossain and D.M. Tow, Phys. Rev. D14 (1976) 3141.
[50] R.G. Roberts, Nucl. Phys. B116 (1976) 334.
[51] Tsou S.T., Phys. Rev. D16 (1977) 2353.
[52] C. Quigg and E. Rabinovici, Phys. Rev. D13 (1976) 2525.
[53] G. Veneziano, Nucl. Phys. B117 (1976) 519.
[54] P. Aurenche and L. Gonzalez-Mestres, Orsay preprint LPTHE 77/33 (1977).
[55] R. Hong Tuan, Orsay preprint LPTHE 77/28 (1977).
[56] J.N. Dash, S.T. Jones and E.K. Manesis, Marseille preprint 77/p912 (1977) and references therein.
[57] L.A.P. Balazs, Phys. Rev. D15 (1977) 309.
[58] C. Rosenzweig, Phys. Rev. D13 (1976) 3080.
[59] T. Inami, K. Kawarabayashi and S. Kitakado, Phys. Lett. 61B (1976) 60; Prog. Theor. Phys. 56 (1976) 1570.
[60] G.F. Chew and C. Rosenzweig, Phys. Lett. 63B (1976) 429.
[61] J. Millan, Phys. Rev. D15 (1977) 2695.
[62] F. Toyoda and M. Uehara, Prog. Theor. Phys. 57 (1977) 2037.
[63] N.A. Törnquist, Phys. Lett. 64B (1976) 348.
[64] J. Pasupathy, Phys. Lett. 58B (1975) 71; Phys. Rev. D12 (1975) 2929.
[65] H.J. Lipkin, Fermilab Conf. 76/98-THY.
[66] S. Okubo and K. Jagannathan, Phys. Rev. D15 (1977) 177.
[67] Chan H.M., J. Kwiecinski and R.G. Roberts, Phys. Lett. 60B (1976) 367.
[68] M. Fukugita, T. Inami, N. Sakai and S. Yazaki, Nucl. Phys. B121 (1977) 93.
[69] Y. Eylon and J. Finkelstein, Phys. Lett. 66B (1977) 154.
[70] Chan H.M., K. Konishi, J. Kwiecinski and R.G. Roberts, Phys. Lett. 60B (1976) 469.
[71] J. Kwiecinski, Phys. Lett. 72B (1977) 245.
[72] E. Berger and C. Sorensen, Phys. Lett. 62B (1976) 303.
[73] C. Sorensen and D.M. Webber, Nucl. Phys. B122 (1977) 331.
[74] For interesting recent work see S. Yazaki, M. Fukugita, T. Inami and N. Sakai, Phys. Lett. 68B (1977) 251; and M. Bishari, F. Hayot, U. Maor and H. Navelet, Saclay preprint DPh T-77/96.
[75] Chan H.M., K. Konishi, J. Kwiecinski and R.G. Roberts, Phys. Lett. 64B (1976) 301.
[76] J. Uschersohn, Nucl. Phys. B114 (1976) 137.
[77] Chan H.M., K. Konishi, J. Kwiecinski and R.G. Roberts, Phys. Lett. 63B (1976) 441.
[78] K. Konishi and J. Kwiecinski, Nucl. Phys. B119 (1977) 210.
[79] P. Zenczykowski, Jagellonion University preprint TPJU-16/77 (April 1977).
[80] G.F. Chew and C. Rosenzweig, Phys. Rev. D15 (1977) 3433.
[81] J.L. Rosner, Phys. Rev. Lett. 21 (1968) 950.
[82] S. Flatté and C. Rosenzweig, in: Proc. 1977 Meeting of the Division of Particles and Fields, APS conference series, Argonne National Laboratory.
[83] G.F. Chew, Lawrence Berkeley Laboratory report LBL-5391 (1976) and in: Proc. 3rd European Symposium on $N\bar{N}$ interactions, Stockholm, 1976;
C. Rosenzweig, Phys. Rev. Lett. 36 (1976) 697.
[84] P.G.O. Freund, R. Waltz and J.L. Rosner, Nucl. Phys. B13 (1969) 237;
M. Imachi, S. Otsuki and F. Toyoda, Prog. Theor. Phys. 55 (1976) 551; 57 (1977) 517;
G.C. Rossi and G. Veneziano, Nucl. Phys. B123 (1977) 507;
K. Konishi, Nucl. Phys. B131 (1977) 143;
F. Toyoda and M. Uehara, Prog. Theor. Phys. 58 (1977) 1456;

C. Rosenzweig, Phys. Lett. 71B (1977) 203;
T. Inami, K. Kawarabayashi and S. Kitakado, Phys. Lett. 72B (1977) 127;
N. Papadopolous, ETH preprint (1977).
[85] H.P. Stapp, Lawrence Berkeley Laboratory report LBL-6735 (1977).
[86] G.F. Chew, J. Finkelstein, J.P. Sursock and G. Weissmann, Lawrence Berkeley Laboratory report LBL-7237 (1977).
[87] M. Imachi, S. Otcuki and F. Toyoda, Progr. Theor. Phys. 54 (1975) 280 and references therein.